The apparent explosion moment: Inferences of volumetric moment due to source medium damage by underground nuclear explosions

Howard J. Patton[1] and Steven R. Taylor[2]

Received 16 August 2010; revised 10 December 2010; accepted 3 January 2011; published 25 March 2011.

[1] Classical explosion source theory relates isotropic seismic moment to the steady state level of the reduced displacement potential. The theoretical isotropic moment for an incompressible source region M_t is proportional to cavity volume V_c created by pressurization of materials around the point of energy release. Source medium damage due to nonlinear deformations caused by the explosion will also induce volume change V_d and radiate seismic waves as volumetric, double-couple, and compensated linear vector dipole (CLVD) body force systems. A new source model is presented where K is a relative measure of moment M_{CLVD} with respect to the net moment from volumetric sources V_c and V_d. K values from moment tensor inversions steadily decrease from ~2.5 at lower yields to ~1.0 for the highest-yield shots on Pahute Mesa. A value of 1.0 implies $M_{CLVD} = 0$ and, by inference, small V_d. We hypothesize that the extent to which damage adds (or subtracts) volumetric moment is controlled by material properties and dynamics of stress wave rebound, shock wave interactions with the free surface, gravitational unloading, and slapdown of spalled near-surface layers. This hypothesis is tested by comparing measurements of isotropic moment $\hat{M}_I$ with estimates of M_t based on V_c scaling relationships and velocity-density models. The results support the hypothesis and the conclusion that $\hat{M}_I$ represents the "apparent explosion moment" since it has contributions from direct effects due to cavity formation and indirect effects due to material damage. Implications for yield estimation using $\hat{M}_I$ are discussed in general and for the North Korean tests.

Citation: Patton, H. J., and S. R. Taylor (2011), The apparent explosion moment: Inferences of volumetric moment due to source medium damage by underground nuclear explosions, *J. Geophys. Res.*, *116*, B03310, doi:10.1029/2010JB007937.

1. Introduction

[2] An equivalent body force representation for the earthquake source was understood in the early years of quantitative seismology after controversies surrounding single- and double-couple force models were resolved in the 1960s. Unlike the relatively quick resolution for earthquakes, controversies surrounding the appropriate body force representation for explosion sources have dragged on for decades. In the wake of successes modeling earthquakes with double couples, tectonic release models for nuclear explosions were developed in the 1970s and 1980s involving a linear superposition of monopole and double-couple force systems. It came as a surprise to explosion seismologists when such models gave estimates of isotropic seismic moment that did not correlate with explosion yield as well as yield estimates based on m_b [*Ekström and Richards*, 1994]. Nor do they answer conundrums surrounding the m_b-M_s discriminant [*Stevens and Day*, 1985] (for example, why do explosion observations not show a slope of 1.0 on a plot of m_b versus M_s, as predicted by the *Mueller and Murphy* [1971] model?) Something fundamental was missing in explosion source descriptions where the only contributor to source asymmetry was tectonic release represented by a double-couple force system.

[3] The effects of a free surface significantly modify near-source phenomenology beyond what is predicted by classical explosion source models developed for an infinite homogeneous medium [*Sharpe*, 1942; *Mueller and Murphy*, 1971, hereafter MM71]. The direct effects of buried nuclear explosions including cavity formation and a heavily damaged surrounding shatter zone [*Bishop*, 1963] are well known and have been well studied. Indirect effects related to shock wave interactions with the free surface and stress wave rebound at depth are also well known, but an integrated view of their significant deformations in the surrounding medium has not been adequately accounted for in previous source models. An example is the model for spallation over ground zero which failed to predict an effect of tensile failure on Rayleigh wave radiation [*Day and McLaughlin*, 1991].

[4] Recently, the work of *Ben-Zion and Ampuero* [2009] raises the possibility of significant seismic radiation from material damage in the source medium associated with brittle deformation. They claim that contributions of damage

[1]Los Alamos National Laboratory, Los Alamos, New Mexico, USA.
[2]Rocky Mountain Geophysics, Los Alamos, New Mexico, USA.

0148-0227/11/2010JB007937

to the radiation from earthquakes can be comparable to or larger than the contribution of moment release due to slip on earthquake faults. Material damage has long been recognized by explosion and earthquake seismologists as a potential source, and models for the seismic radiation have been developed over the years [e.g., *Mal and Knopoff*, 1967; *Knopoff and Randall*, 1970; *Ashby and Sammis*, 1990; *Johnson and Sammis*, 2001; *Taylor*, 2009]. Among the predictions of these models is the fact that source medium damage can radiate waves as volumetric, double couple, and compensated linear vector dipole (CLVD) body force systems. The role that damage might play in seismic radiation from explosions sources has implications for source discrimination, for yield estimation, and for the physical basis of shear wave generation from buried explosions.

[5] In this paper, an explosion source model is presented that follows up the study of *Patton and Taylor* [2008]. In that study, a CLVD body force system was introduced into a tectonic release model for purposes of explaining m_b-M_s observations of the 2006 North Korean nuclear test. The results demonstrated the very significant impact that Rayleigh wave radiation from the CLVD can have on M_s and on the performance of the m_b-M_s discriminant. Here we consider another long-period effect of source medium damage since it can contribute not only to the deviatoric source but also to the equivalent volumetric source of buried explosions.

2. An Explosion Source Model Accounting for Source Medium Damage

[6] The motivation for a source damage model comes from studies of many investigators, some that were summarized in the Introduction. In addition to an understanding of microscopic damage from such studies, numerical simulations of hydrodynamic flow in realistic materials [e.g., *App and Brunish*, 1992; *Jones et al.*, 1993] and their implications for damage on macroscopic scales have had a great influence on our work. We begin this section with an idealized description of source phenomenology on the time scale of 1 s after an underground explosion occurs. This description captures the salient features seen in these numerical simulations and serves to lay a physical basis for a source model that includes the effects of material damage. An equivalent elastodynamic representation for damage is discussed later in this section.

[7] The dynamics of source processes related to damage are illustrated in Figure 1 with a series of time snapshots or frames showing schematic cross sections through the source region. Time progresses across Figure 1 from preshot conditions through spall slapdown in eight time steps. Time is provided in each frame as an approximate guide for the occurrence of certain key phenomena under emplacement conditions where the depth of burial is 300 m and P wave velocity is 3000 m/s. The future cavity formed by the explosion is depicted in each frame and serves as a reference point. The reader should consult the caption of Figure 1 for definitions of features used in these schematics.

[8] Outgoing strong shock waves (frame 2 in Figure 1) damage the medium causing a shatter zone (frame 3 in Figure 1) around the point of energy release. Communication with the free surface results in reflected waves that start to set up a tensile regime at shallow depths (frame 4 in Figure 1), where the conditions for spallation [*Viecelli*, 1973] are first met. Hydrodynamic flow returning toward the source, called "shock or stress wave rebound," is seen first at depth where impedance is highest. Rebound is one of the drivers of subsequent material damage as time progresses. In frame 5 in Figure 1, more heaving and initial bulking occurs at shallow depths, while the first signs of rotations in the medium on macroscopic scales are seen at greater depths. Propagation through the shatter zone attenuates and possibly delays the downgoing *pP* [*Douglas and Hudson*, 1990; *Lay*, 1991].

[9] Incipient spall in frame 5 in Figure 1 reaches greater depths in frame 6, causing vertical parting of horizontal layers. Mechanical communication between the layers during spall still exists through layer collisions. Detachment is finite in depth and in time, as is spall slapdown. Frames 6 and 7 in Figure 1 illustrate how gravitational unloading facilitates rotational motions and shock wave rebound inward and upward causing heaving and bulking at depth over the shot point. Rotational motions on microscopic and macroscopic scales lead to the development of slip planes on the margins of a conical volume and facilitate bulking of the medium through rubblization and block motions within the volume. Frame 8 in Figure 1 depicts slapdown of spalled layers and more radiation of shock waves in the atmosphere and in the solid Earth. The impulse of slapdown is proportional to the mass and velocity of spalled material when it impacts the ground. This impulse compacts the medium, and if it is strong enough, reverses displacement on the slip planes and crushes the material matrix in which void spaces were created earlier in the failure process.

2.1. Elastodynamic Representations of Damage on Buried Explosions

[10] In addition to direct effects of strong shocks creating a shatter zone of severely damage material, driving forces of the model include the dynamics of stress wave rebound, shock wave interactions with the free surface, gravitational unloading, and subsequent slapdown of spalled near-surface layers and their effects on the source medium. It can be debated which is more important: "taffy pull" of the free surface dynamics and subsequent tensile stresses or "tube of toothpaste squeeze" of the stress wave rebound. In any case, the source medium undergoes various modes of failure and suffers changes in both bulk and shear material properties. In light of the estimates of damage occurring on earthquakes [*Ben-Zion and Ampuero*, 2009], the contribution of damage to seismic radiation from explosions must be significant and accounted for in new models of the source.

[11] *Patton and Taylor* [2008, hereafter PT08] proposed a damage model for shock-induced, deep-seated tensile failure that identified extensional deformations along a vertical axis of symmetry and contractions around the waist of the explosion as a cause of damage. Such deformations can be seen in the hydrodynamic flow in frames 5–7 in Figure 1. A complete phenomenological description of damage is more complex than PT08's model since many modes of failure are involved, including those related to spall slapdown. Nevertheless, this model serves as our point of departure for an elastodynamic description of damage, where a compensated linear vector dipole CLVD in extension along the vertical axis is one constituent body force system of the model.

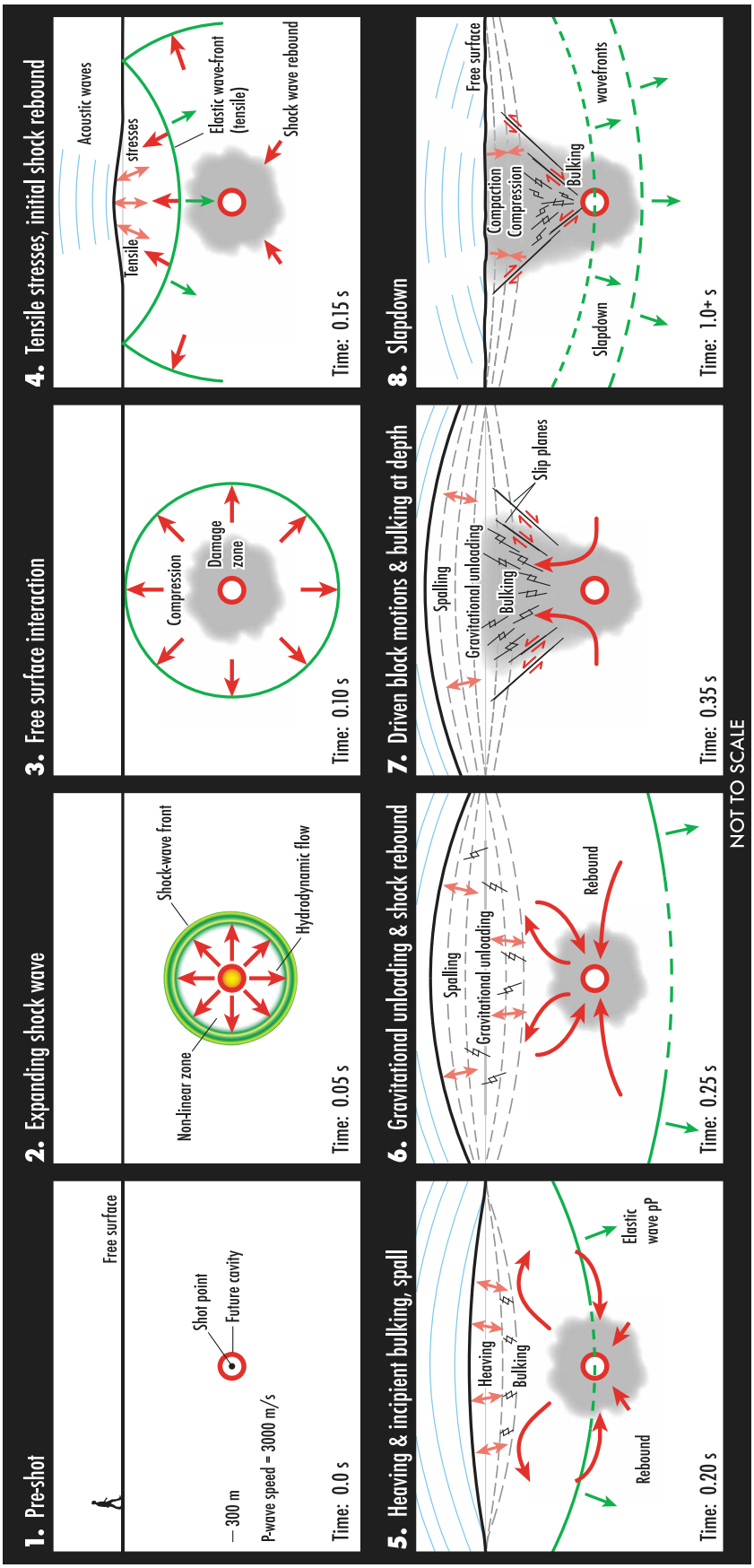

Figure 1. Dynamics of explosion source processes in eight time frames from preshot to spall slapdown. Heavy red arrows denote hydrodynamic or material flow in the source medium, double light red arrows denote compressive or tensile stresses, red coupled arrows indicate driven slip on faults, green lines in frame 3 and onward indicate elastic wavefronts, green arrows indicate direction of *P* wave propagation, blue lines indicate acoustic wavefronts in the atmosphere, gray dashed lines indicate substrata undergoing heaving and spallation, shaded areas indicate source medium suffering material damage, ratchets denote bulking, and a heavy solid black line indicates the free surface. The red circle is the explosion cavity.

[12] The motivation behind a CLVD representation comes from theoretical [*Knopoff and Randall*, 1970; *Ben-Zion and Ampuero*, 2009] and modeling studies [*Stevens et al.*, 2003; *Patton et al.*, 2005]. Using the representation theorem for seismic sources, model C of *Knopoff and Randall* [1970] investigates a sudden change of shear modulus $\Delta\mu$ in the presence of axial strain. Assuming uniaxial strains along the vertical axis, *Knopoff and Randall*'s [1970] formulation predicts the P wave radiation in terms of a strain jump Δe_{zz} accompanying brittle deformation

$$u_k = -2\Delta\mu\Delta e_{zz} V_s \cdot \frac{\partial G_{kz}}{\partial \xi_z}, \tag{1}$$

where V_s is the source volume, ξ_z is the z source coordinate, and a Green's function G_{kz} is the kth component of displacement due to a unit point force acting in the z direction. $\partial G_{kz}/\partial \xi_z$ is a vertical dipole force. *Ben-Zion and Ampuero* [2009] point out that the proper representation involves total elastic strains relative to the initial strain state of the source medium, not a strain jump Δe_{zz}; that is, Δe_{zz} in equation (1) should be replaced by e_{zz}, the total elastic strain along the vertical axis. A similar result is obtained for a sudden change in Lamé's coefficient λ. A linear vector dipole is characterized by zero net force, zero net momentum (linear and angular), and a net volume change.

[13] Moment tensor decompositions can relate a vertical dipole force M_{zz} to a CLVD force system as implemented in the model of PT08, where it is understood that the first-order moment tensor M_{ij} is symmetric with the form

$$\begin{bmatrix} M_{xx} & M_{xy} & M_{xz} \\ M_{yx} & M_{yy} & M_{yz} \\ M_{zx} & M_{zy} & M_{zz} \end{bmatrix}. \tag{2}$$

The decomposition of M_{zz} with unit source strength can be written as follows

$$\begin{bmatrix} 0 & 0 & 0 \\ 0 & 0 & 0 \\ 0 & 0 & 1 \end{bmatrix} = \frac{1}{3}\begin{bmatrix} 1 & 0 & 0 \\ 0 & 1 & 0 \\ 0 & 0 & 1 \end{bmatrix} + \frac{2}{3}\begin{bmatrix} -0.5 & 0 & 0 \\ 0 & -0.5 & 0 \\ 0 & 0 & 1 \end{bmatrix}, \tag{3}$$

where the first term on the right is an isotropic volumetric source with strength 1/3, which is one half the strength of a CLVD with a vertical axis of symmetry in extension in the second term. This model can be regarded as making two contributions to the radiated seismic wavefield, one due to a volumetric source and one from a deviatoric source in the form of a CLVD. As mentioned above, a model for damage can include radiation from all three source types: volumetric and a general deviatoric source composed of double-couple and CLVD body force systems.

[14] The deviatoric source in equation (3) was explicitly written into PT08's model. The volumetric source of this model consists of two contributions, one from cavity formation and the other from nonlinear failure mechanisms occurring in an inverted conical source volume over the shot point, illustrated schematically in Figure 1. Thus, isotropic moment must be regarded as "apparent" explosion moment due to direct and indirect volumetric effects in the source medium of the explosion.

2.2. An Explosion Source Model With Damage

[15] Following PT08, the model is composed of a linear superposition of three body force systems: three orthogonal dipole forces of equal strength representing the spherical or monopole source, a double couple for relaxation of tectonic prestress, and a CLVD with vertical axis of symmetry for the deviatoric contribution of source medium damage. To first order, the CLVD is expected to have a vertical axis of symmetry in extension provided that topography over ground zero is not very great. The reason is that the T axis of the CLVD should align along the direction of minimum compressive stress, and this direction is dictated by explosion dynamics due to tensile stresses set up by rarefactions off the free surface. Explosions "sense" the closest approach to the free surface owing to the interactions of shock waves establishing a tensile regime.

[16] The style of tectonic release is assumed to be vertical strike-slip faulting which is supported by studies of Pahute Mesa explosions [e.g., *Wallace*, 1991] and mechanisms of nearby shallow seismicity such as the Massachusetts Mountain earthquake located on the eastern boundary faults of Yucca Flats with a focal depth <5 km [*Fischer et al.*, 1972; *Patton*, 1982]. We will discuss an extension to a general double-couple source model for application to other test sites in section 7.

[17] Assuming common time histories, a superposition of explosion, tectonic release, and damage force systems lead to the following expressions for the moment tensor elements

$$\begin{aligned} M_{xx} &= M_I - 0.5 \cdot M_{CLVD} + M_0 \cdot \sin(2\phi) & M_{xy} &= -M_0 \cdot \cos(2\phi) \\ M_{yy} &= M_I - 0.5 \cdot M_{CLVD} - M_0 \cdot \sin(2\phi) & M_{xz} &= 0 \\ M_{zz} &= M_I + M_{CLVD} & M_{yz} &= 0 \end{aligned} \tag{4}$$

where M_I, M_{CLVD}, M_0 are seismic moments for the monopole, CLVD, and double-couple force systems, and ϕ is the strike of a vertically dipping pure right-lateral strike-slip fault. M_I is positive for explosions and negative for implosions, M_{CLVD} is positive for extension along the vertical axis and negative for contraction, and M_0 is always positive.

[18] An index K, analogous to the index F of *Toksöz and Kehrer* [1972] for tectonic release, was introduced by PT08 as a measure of the relative strength of a deviatoric source for damage

$$K \equiv \frac{2M_{zz}}{M_{xx} + M_{yy}}. \tag{5}$$

If relaxation of tectonic stresses occurs only in the horizontal plane, then

$$K = \frac{2(M_I + M_{CLVD})}{2M_I - M_{CLVD}} \text{ and } \frac{M_{CLVD}}{M_I} = \frac{2(K-1)}{K+2}, \tag{6}$$

where M_I is $\mathrm{Tr}[M_{ij}]/3$. A K value of 1 implies a vanishingly small CLVD source. K greater than 1 means the CLVD source has a vertical axis in extension while the horizontal

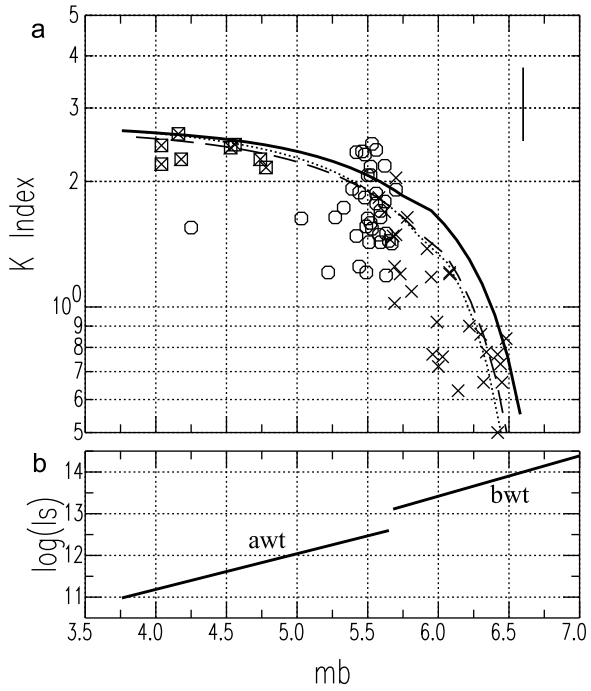

Figure 2. (a) Inferred and measured K values plotted against m_b for NTS explosions on Pahute Mesa. Circles indicate values above the water table (awt); crosses indicate values below the water table (bwt) and Rainier Mesa (crosses enclosed in squares). Lines are inferred curves based on analysis of "A" spectra using the log[W]-m_b relationship of *Vergino and Mensing* [1990] and perturbations thereof (see PT08). An estimate of error bar on measurements of K is shown for reference. (b) Scaling relationships for spall impulse I_s from *Patton* [1990]. An offset occurs due to better coupling for shots below the water table.

dipole forces are in compression. K less than 1 means a vertical axis in compression and horizontal dipole forces in extension. M_{CLVD} is half the size of M_I for a K value of 2.

[19] PT08 showed that at long periods, Rayleigh waves from a vertical CLVD with $K > 1$ destructively interfere with waves excited by the monopole source. This interference occurs on all azimuths and reduces surface wave amplitudes and M_s, making explosions look more explosion-like on a plot of m_b versus M_s. Interference between Rayleigh waves radiated by monopole and CLVD force systems can explain (1) why m_b-M_s observations consistently plot below $M_s = m_b - 1.0$ for m_b less than ~5.5, (2) why the slope of these observations tend to be significantly greater than 1.0 once a systematic dependence of K on yield W is accounted for (see below), and (3) why m_b-M_s observations for the 2006 North Korean test gave unusually large M_s for its m_b (see PT08).

[20] In this paper our focus is on another aspect of long-period radiation: the fact that an explosion suffering source medium damage is expected to have two volumetric sources of radiation. The following is an analysis of moment tensor inversion results for Nevada Test Site (NTS) explosions in which an interpretation of the results is put to a test. A positive outcome constitutes the first time that a significant body of observational evidence supports the hypothesis of a volumetric component due to source medium damage by underground nuclear explosions. It also reinforces the notion of "apparent explosion moment" composed of two volumetric components, one contributed by cavity formation and the other by damage in the surrounding source medium.

3. NTS Results and a Method for Testing Predictions of the Source Model

[21] PT08 analyzed observations of reduced excitation spectra for fundamental mode Rayleigh wave radiation and from this analysis inferred a systematic yield dependence of K. The so-called "A" spectrum [*Patton*, 1988] on which this inference was made is excited by M_{zz} and $M_{xx} + M_{yy}$ dipole force systems only. K measurements for individual NTS explosions were obtained from moment tensor inversion results based on the method of *Patton* [1988, 1991]. This method uses combined data sets of fundamental and higher-mode surface wave spectra for estimates of all six elements of the moment tensor. K values were obtained from equation (5) using estimates of M_{zz} and $M_{xx} + M_{yy}$ from the inversion.

[22] K measurements, along with several inferred curves from PT08, are plotted in Figure 2a as a function of m_b. The curve based on the log[W]-m_b relationship of *Vergino and Mensing* [1990] plots somewhat higher than K measurements above 5.0 m_b. Other curves in Figure 2a show that relatively small perturbations in the *Vergino and Mensing* [1990] relationship can bring them into better agreement with the measurements.

[23] K decreases systematically with increasing yield from an average near 2 at m_b 5.5 to a value less than 1 for the largest tests. Boxcar with an announced W of 1.3 Mt has a K value of 0.7, while Cybar with an announced W of 119 kt has a K value of 2.2. The error bars on K measurements are sizable; nevertheless, there is no question that a decrease in K is real in both the measurements and the inferred curves. Meanwhile, as seen in Figure 2b, the impulse of spall slapdown increases steadily with yield, and undergoes an abrupt increase for shots buried below the water table [*Patton*, 1990]. The gradual decrease in K appears to accelerate for shots below the water table where shock waves couple better into the ground causing more mass to spall with higher velocities than shots above the water table.

[24] A possible explanation why K decreases as W increases was proposed by PT08. A strength threshold for the damaged medium is reached for shots with large enough slapdown impulses. At this point the force of spall slapdown is great enough to crush the material matrix, thereby eliminating void spaces and reversing slip on faults not just at shallow depths as seen in frame 8 in Figure 1, but throughout the damaged volume. This threshold marks the beginning of a reversal process reducing the volume created by bulking and block motions at depth and compacting the material more and more as yield increases. We envision two possible end-member scenarios, one that is typical for most shots while the other is specific to very large shots on Pahute Mesa (Figure 3).

[25] Typically, we expect the medium will show compaction near the free surface since the materials are very weak there (Figure 3, left). At depth, however, the damaged material inside the conical volume remains dilated due to the creation of void spaces and bulking during the deformation processes illustrated in Figure 1. On the other hand for high-

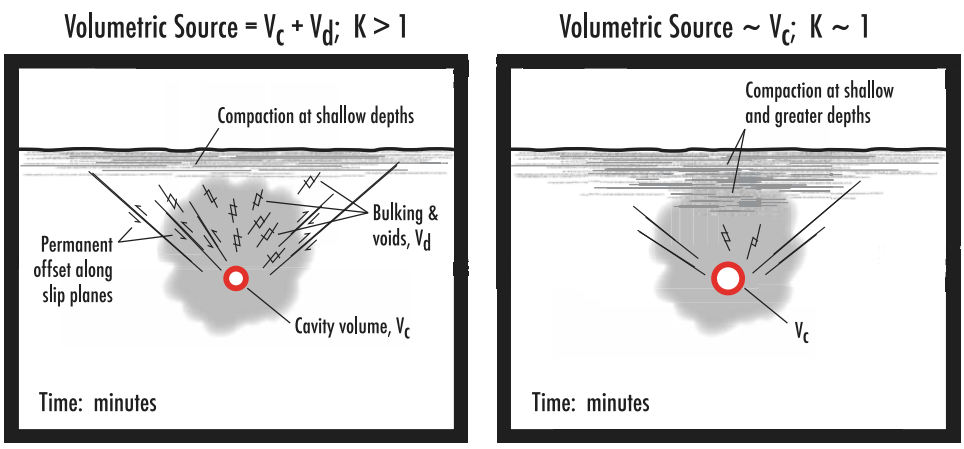

Figure 3. Statics of the explosion source minutes after motions in the source region have subsided. Two scenarios are shown: (left) There is significant bulking and slip on the faults at depth, while compaction is restricted to shallow layers. (right) The impulse of spall slapdown exceeded the strength of the damaged material, crushing the bulked medium, eliminating most voids, reversing slip on faults, and compacting layers to greater depths. Red circle denotes the cavity formed by the explosion, and shaded areas indicate the source volume where significant damage has occurred.

yield shots (Figure 3, right), by exceeding the strength threshold, compaction extends to greater depths, much slip on bounding faults is reversed, and bulking is reduced. Very little volumetric change remains in the damaged material, which can be slightly positive or even negative if net compaction is a larger effect than the residual bulking. Nevertheless, the cavity volume remains intact in both scenarios owing to the containment cage that forms around the cavity due to sealing effects of hoop stresses [*U.S. Department of Energy*, 1995, chapter 11].

[26] In summary, damage to the source medium by explosions can introduce another volumetric source in addition to the cavity creation. However, the dynamics of source processes are such that spall slapdown could reverse some or all of the volume's dilation, even to the point of contracting the source medium's volume for porous media. Our hypothesis for the behavior of K is that the volumetric component for the largest Pahute Mesa shots is due mainly to cavity formation, while most smaller shots should have an additional volumetric component due to failure processes over the shot point.

[27] Using classical theory, estimates of seismic moment M_t based on cavity volume are made for ~65 explosions detonated on Pahute Mesa. Comparisons will be made between M_t and measurements of M_I, denoted $\hat{M}_I$. If the hypothesis is correct, $\hat{M}_I$ should be larger than M_t for most shots, but the difference will decrease for shots of increasing yield below the water table and should vanish or might even reverse sign such that M_t is greater than $\hat{M}_I$ for very large shots.

4. Seismic Moment for the Classical Explosion Source Model

[28] *Sharpe* [1942] obtained a solution for waves generated by sudden pressurization of a spherical cavity imbedded in a homogeneous elastic whole space. This solution is written in terms of a reduced displacement potential $\psi(\tau)$ acting on an "elastic sphere," where τ is reduced time $t - r/\alpha$, r is radial distance from the center of the sphere and α is the speed of P waves in the medium. The concept of an elastic radius r_e ($\gg r_c$, the cavity radius) is used to denote a distance at which expanding pressure waves exceeding the elastic limit are reduced in amplitude to the point where linear elastic theory applies.

[29] Of interest is the steady state solution of this source. At the elastic radius r_e, theory relates the static pressure ΔP and permanent radial displacement Δu_r. The relationship may be found by taking the limit as $\tau \rightarrow \infty$ of equation 9 of *Denny and Johnson* [1991, hereafter DJ91] for $\psi(\tau)$ and solving for Δu_r ($= -\partial[\psi(\infty)/\mathrm{r}]/\partial \mathrm{r}$) at r_e,

$$\Delta P = \frac{4\mu \cdot \Delta u_r}{r_e}, \tag{7}$$

where μ is the medium's shear modulus, and $\psi(\infty)$ is called the static or residual potential. Using the representation theorem [*Aki and Richards*, 2002, equations 3.3 and 3.24], the body force equivalent of a spherical source is three mutually perpendicular dipole forces of equal moment M [see *Aki and Richards*, 2002, problem 3.8]

$$M = \pi\left(\frac{\rho\alpha^2}{\mu}\right) \cdot r_e^3 \Delta P, \tag{8}$$

where ρ is source medium density, and $\rho\alpha^2$ is sometimes referred to as the acoustic bulk modulus (e.g., that portion of the bulk modulus = $\rho[\alpha^2 - (4\beta^2/3)]$ related to compression, where β is shear wave velocity). Substituting for ΔP yields the equation first derived by *Müller* [1973],

$$M = \rho\alpha^2 \cdot S_e \Delta u_r = (\lambda + 2\mu) \cdot S_e \Delta u_r, \tag{9}$$

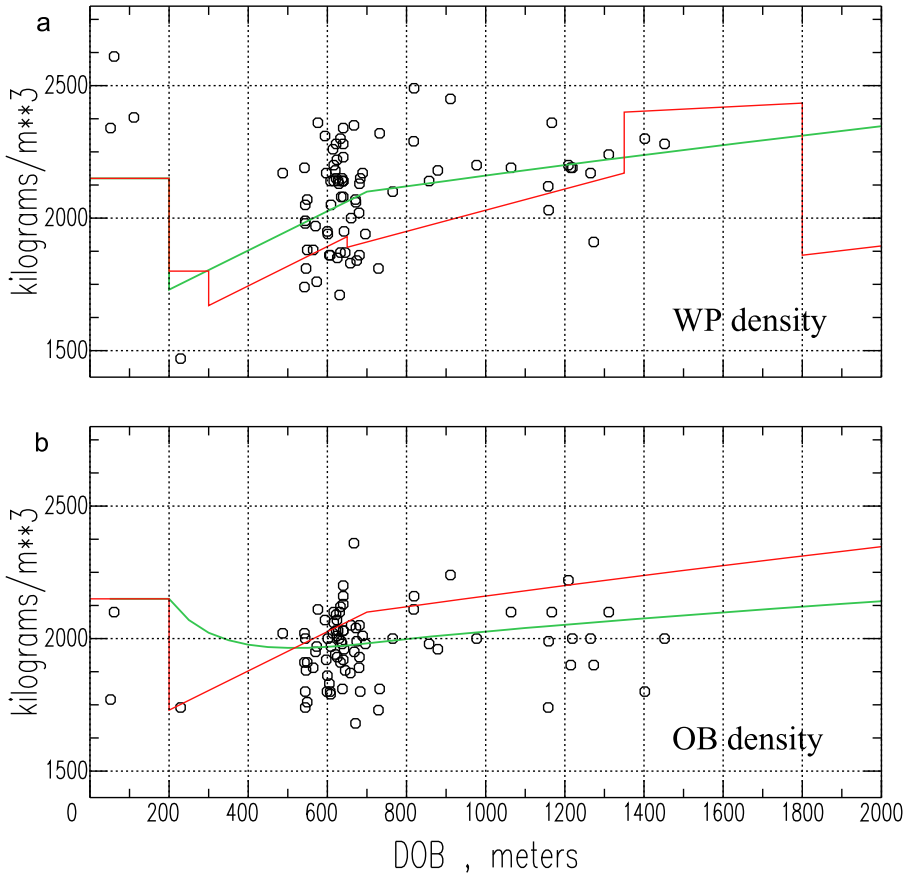

Figure 4. (a) Measurements of working point (WP) density in kg/m^3 for explosions on Pahute Mesa along with a density–depth of burial (DOB) profile based on the results of *Ferguson et al.* [1994] (red) and the WP density model (green) adopted in this study. The latter profile consists of a constant density surface layer 200 m thick and three linear segments (200–700 m, 700–1350 m, and 1350–3000 m). (b) Estimates of overburden density in kg/m^3 along with the overburden OB density profile (green) calculated from the WP density model (red).

where S_e is surface area of the elastic sphere. The similarity of this equation to *Aki*'s [1966] famous equation for the seismic moment of earthquakes ($M_0 = \mu\Sigma d$, where Σ is area of the ruptured fault plane and d is mean dislocation on the fault) is striking. Note that for small Δu_r compared to r_e, $S_e\Delta u_r$ represents a net volume change. Under the assumption that compressibility of the nonlinear region around the source is negligible, this volume change equals the volume V_c created by pressurization of a hollow cavity around the point of detonation (see MM71, p. 1679). We use M_t to denote the volumetric moment associated with cavity creation, and its formula follows from equation (9).

$$M_t = \rho\alpha^2 \cdot V_c. \tag{10}$$

For a review of equation (9)'s validity for explosive sources and the extension to equation (10), the reader should see *Richards and Kim* [2005], *Aki et al.* [1974], and MM71.

[30] As an aside, it is interesting to note that equation (10) is sometimes viewed as an upper bound on explosion moment since source medium compaction caused by radiated shock waves and spall slapdown should reduce the final or static displacement on the elastic radius [MM71; *Murphy*, 1974; *Aki et al.* 1974; *Aki and Bouchon*, 1974; *Murphy*, 1977]. *Murphy* [1974] employed this equation with a cavity radius scaling relationship and found that [*Murphy*, 1974, p. 1596] "estimates of the seismic moment for events in tuff based on close-in data (i.e., cavity radius) are remarkably consistent with those obtained from long-period Rayleigh waves." Apparently the effects of material compaction were small after all; cavity radius scaling could be used to predict explosion moment over the objections of *Aki et al.* [1974] who uncovered discrepancies between $\hat{M}_I$ obtained from long-period Rayleigh waves and moments based on cavity radius and residual potential $\psi(\infty)$ measurements. The present study will shed more light on the classical interpretation of moment and the role of source medium dilation due to damage, which apparently neither *Murphy* [1974] nor *Aki et al.* [1974] considered.

5. Shallow Earth Structure and Scaling Relationships for Cavity Radius on Pahute Mesa

[31] There are two major ingredients needed to estimate M_t with equation (10): acoustic bulk modulus $\rho\alpha^2$ and cavity volume V_c. This section describes the data and methods that were utilized to arrive at our estimates of these quantities. For M_t based on surface waves, we seek a smooth

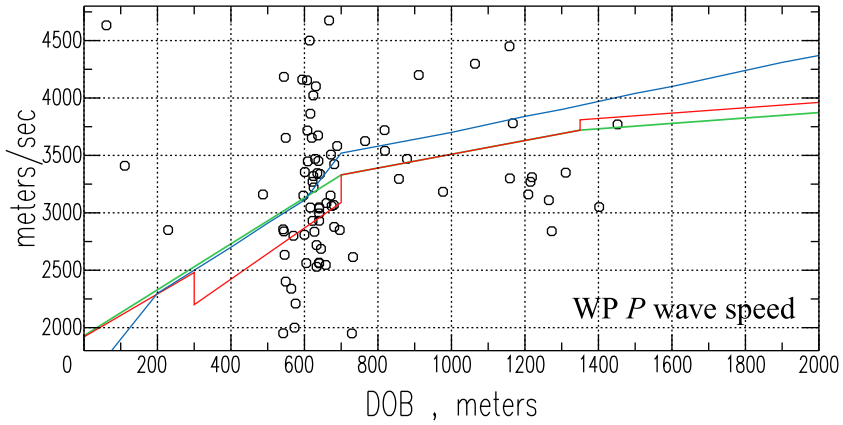

Figure 5. Models of WP *P* wave speed in m/s as a function of DOB, plotted with measurements for explosions on Pahute Mesa. Red profile is based on the results of *Ferguson et al.* [1994], blue profile is based on the study of *Leonard and Johnson* [1987], and green profile is the WP *P* wave speed model adopted in this study consisting of three linear segments (0–700 m, 700–1350 m, and 1350–2500 m).

variation with depth of $\rho\alpha^2$ representing an average acoustic bulk modulus on the elastic sphere. This will be accomplished by integrating density and *P* velocity profiles over the depth range $h - r_e$ and $h + r_e$, where h is the depth of burial. Due to the classified nature of cavity radius r_c and yield W data, we cannot report the actual measurements of r_c and W for shots in our data set. Rather, we first develop a scaling relationship for the ratio $r_c/W^{1/3}$ using classified data sources. Assuming standard burial practice (e.g., $h = 120 \cdot W^{1/3}$), the ratio h / 120 is used as a surrogate for $W^{1/3}$ in the derived relationship in order to estimate the variation of r_c with h.

[32] For estimates of $\rho\alpha^2$, we draw on key references for density [*Ferguson et al.*, 1994] and *P* wave velocity [*Leonard and Johnson*, 1987] on Pahute Mesa. *Ferguson et al.* [1994] provide density- and velocity-depth profiles for a transect across the Silent Canyon caldera complex through NTS testing areas 19 and 20. The transect is based on borehole logs and seismic data recorded on tests in our data set along with other seismic and gravity data collected for mapping volcanic stratigraphy and geologic structure in the upper 5 km.

[33] Figure 4a shows working point (WP) densities measured on shots across the two areas from *Springer et al.* [2002] along with a density profile developed by *Ferguson et al.* [1994] for a point on the transect 20 km from the northwestern end. This point lies near 37.27°N and 116.40°E, close to the boundary of areas 19 and 20. The density profile consists of five linear segments to a depth of 2000 m. We modified their profile to fit through the WP measurements better by adopting a four segment model consisting of a constant density layer in the top 200 m, a linear profile between 200 and 700 m with the same slope 0.74 kg/m^3/m as their third segment, and two more segments with reduced slopes similar to their model below 1800 m.

[34] An overburden (OB) density profile was obtained by integrating the model WP density profile and dividing by depth. The resulting profile is shown in Figure 4b along with estimates of OB density for shots on Pahute Mesa. The WP model does a good job predicting OB densities on these shots.

[35] Turning to *P* wave velocities, *Leonard and Johnson* [1987] and *Ferguson et al.* [1994] developed travel time curves for the Silent Canyon caldera complex from nuclear tests and a wide-angle seismic survey for imaging deeper structures. Inversions of these travel time curves resulted in the models shown in Figure 5. WP measurements of velocity for Pahute Mesa shots [*Springer et al.*, 2002] are plotted for comparison and show a large spread. One standard deviation measurement errors are typically ~20% for WP velocity [*Howard*, 1985]. This spread in WP velocities (as well as WP densities) illustrates why it would be unwise to use actual measurements to estimate the acoustic bulk modulus on a shot by shot basis. Rather, we elected to use models that are better representations of the average properties. Furthermore, the initial *P* radiation that eventually goes on to form Rayleigh waves samples the entire elastic sphere. So the acoustic bulk modulus should represent the average properties over the sphere.

[36] The *Ferguson et al.* [1994] model (for the same sample point on the transect as the density model above) has a slight velocity inversion at depths between 300 and 700 m. Otherwise it compares well with the results of *Leonard and Johnson* [1987]. The model we adopted follows *Leonard and Johnson* [1987] very closely in the top 700 m, but favors *Ferguson et al.* [1994] at greater depths where it is believed that their model is more reliable than that of *Leonard and Johnson* [1987]. *Ferguson et al.* [1994] included data from a wide-angle seismic survey which helped constrain velocities at depth better. Our model consists of three linear segments extending to 2500 m, with a gradient of 2 m/s/m in the top 700 m, decreasing to 0.6 and 0.235 m/s/m in the lower two segments.

[37] Figure 6 shows two depth profiles of acoustic bulk modulus and sample points based on measurements of WP density and velocity for Pahute shots. The profiles were obtained with two different methods. The first method is simply the product of WP density and velocity-squared profiles presented above. The second method averaged $\rho\alpha^2$ on the elastic sphere using the formula

$$avg\left[\rho\alpha^2\right] = \frac{1}{2r_e}\int_{h+r_e}^{h-r_e}\left[\rho(z)\cdot\alpha(z)^2\right]dz, \qquad (11)$$

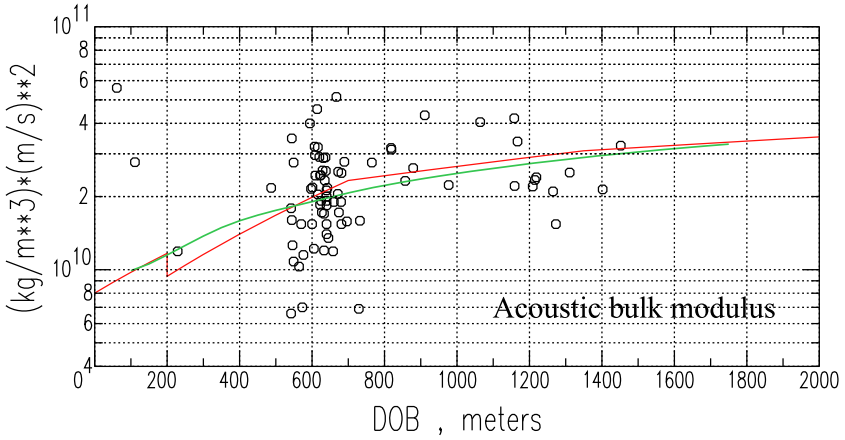

Figure 6. Models of acoustic bulk modulus ($\lambda + 2\mu$) as a function of DOB, plotted with point estimates of $\rho\alpha^2$ using measurements of WP density and P wave speed for shots on Pahute Mesa. Red profile is based on adopted WP density and velocity models in Figures 4 and 5, respectively. Green profile represents the average acoustic bulk modulus on a sphere with its center at depth h and a radius equal to r_e.

where $\rho(z)$ and $\alpha(z)$ are WP profiles depending on depth z only. An estimate of r_e is found using the $r_c(h)$ relationship developed in the next paragraph and multiplying this radius by a factor of 10 (DJ91). In cases where $r_e > h$, the integration was stopped at the free surface. The result of this averaging is a smoothed version of the former profile based on WP models.

[38] In general, both profiles pass near the centroid of sample points in the depth range where most Pahute explosions were detonated. The averaged curve for acoustic bulk modulus depends on depth of burial, and a fit with a power law model gives $\sim h^{0.5}$ for depths greater than ~300 m.

[39] To develop a relationship for r_c, we adopted a parameterization similar to DJ91's equation (39). The effect of gas porosity (GP) on r_c was found to be very small, and indeed DJ91 found that observations of r_c for explosions in hard rock and porous media overlay after correcting for the other parameters. Since average WP GP for Pahute shots is only 4% and individual measurements never exceed 12%, we decided to omit GP in the parameterization. Furthermore, it was too much to ask the data set of ~80 Pahute Mesa shots to resolve the effects of material strength, measured by shear velocity β, from the effects of overburden P_0 (ρgh, where g is gravitational acceleration). Thus we adopted quarter-root scaling on P_0, as *Boardman et al.* [1964] did, which is not very different from the scaling exponent (0.2625) determined by DJ91 from a much larger data set. The parameterization used in our study is

$$r_c = \frac{C \cdot W^{1/3}}{\beta^x \cdot P_0^{1/4}}, \tag{12}$$

where C and x are unknown constants to be determined by the observations. We solved for these constants by simple least squares using a model equation of the form, $\log[y] = \log[C] - x \cdot \log[\beta]$, where $y = r_c \cdot (P_0)^{1/4}/W^{1/3}$. Measured OB densities for individual shots along with their burial depths [*Springer et al.*, 2002] were used to compute P_0 while β is based on our WP velocity model for P waves where a Poisson ratio ν of 0.3 is assumed. The least squares inversion gave values for $x = 0.612 \pm 0.280$ and for $\log[C] = 4.798 \pm 0.907$ or $C = 6.28 \times 10^4$ in MKS units.

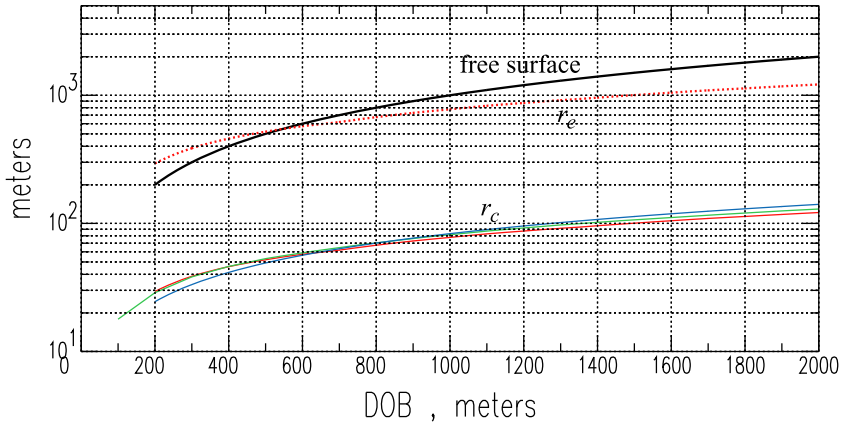

Figure 7. Predictions of r_c as a function of DOB based on the results of this study (red), DJ91 (green), and *Heard and Ackerman* [1967] used by MM71 (blue). r_e (dotted red) is a factor of 10 greater than r_c from this study. The elastic sphere is completely subterranean for shots buried at depths greater than 550 m.

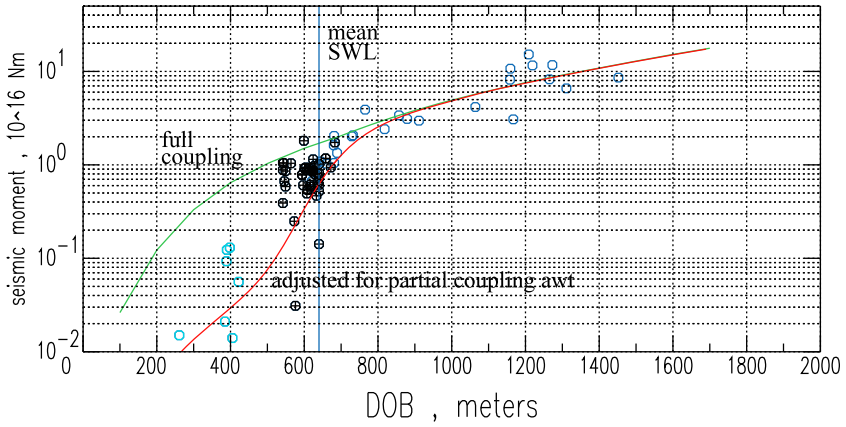

Figure 8. Computed explosion moment M_t and $\hat{M}_I$ for explosions on Pahute Mesa. Green curve is M_t for full coupling at all depths, while the red curve is M_t adjusted for the effects of surface wave coupling. The vertical blue line represents the mean standing water level SWL on Pahute Mesa (640 m). Open blue circles are $\hat{M}_I$ for shots located below the SWL determined for that specific emplacement hole, and likewise for shots above the SWL shown with pluses enclosed by black circles. Cyan open circles are explosions detonated in tunnels beneath Rainier Mesa.

[40] Classification prohibits our use of official yields to compute cavity radius. Instead, estimates of r_c are computed as a function of depth of burial assuming standard containment practice as a surrogate for yield. The relationship for r_c becomes

$$r_c = \frac{6.28 \times 10^4 \cdot (h/120)}{\beta^{0.612} \cdot P_0^{1/4}} = \frac{434 \cdot h^{0.75}}{\alpha^{0.612} \rho^{0.25}}, \qquad (13)$$

where α is WP velocity plotted in Figure 5 and ρ is OB density plotted in Figure 4b. Figure 7 shows this relationship plotted against burial depth h along with r_c predicted by DJ91 and *Heard and Ackerman* [1967] assuming standard containment practice and ignoring the effects of gas porosity. Also plotted is r_e, assuming $r_e \sim 10 \cdot r_c$. Note that under these assumptions, r_e intersects the free surface for burial depths less than ~550 m under standard containment practices.

6. Comparisons of $\hat{M}_I$ and Classical Seismic Moment M_t

[41] Having obtained estimates for the average acoustic bulk modulus as a function of source depth (Figure 6) and cavity radius r_c in equation (13), the two basic ingredients for estimating classical seismic moment M_t are determined by use of equation (10). The results are plotted in Figure 8 along with $\hat{M}_I$ for Pahute Mesa explosions. These measurements were obtained from moment tensor inversions of regional surface wave data using the method of *Patton* [1988, 1991] for 57 explosions and the full waveform modeling method of *Ford et al.* [2009] for an additional 7 explosions.

[42] On average, estimates of M_t agree well with $\hat{M}_I$ for large deep Pahute Mesa explosions. As depths shallow, however, the estimates of M_t become higher. The reason is that seismic coupling is reduced for dry porous media above the water table, in contrast to the good coupling characteristics for water saturated media below the water table. The average depth of the water table on Pahute Mesa is 640 m, and M_t starts to differ systematically from $\hat{M}_I$ as source depths approach and cross the water table. To make the comparison between M_t and $\hat{M}_I$ valid over the entire depth range, seismic coupling variations as a function of depth must be accounted for.

[43] *Taylor* [1982] developed coupling factors for 10 s Rayleigh waves recorded on the four broadband stations operated by Lawrence Livermore National Laboratory, while *Jones and Taylor* [1996] used a more extensive data set of NTS explosions to develop *Lg* coupling factors using a technique similar to that of *Taylor* [1982; see *Jones and Taylor*, 1996, Figure 11b]. Coupling factors for both data sets have units proportional to the logarithm of amplitude per kiloton and are in good agreement except for depths shallower than 600 m. The Lg data set was considered more reliable at shallow depths due to concerns about censoring bias for Rayleigh measurements at low yields. We combined the data sets using Rayleigh wave coupling measurements for deep shots on Pahute Mesa, which were not included in the *Lg* data set of *Jones and Taylor* [1996]. The combined data sets were fit with a sigmoid function of the form

$$f(z, a, b, c, d) = d + \frac{a}{1 + e^{-b(z-c)}}, \qquad (14)$$

where z is the depth (m), a controls the amplitude, b controls the gradient, c the inflection point, and d the initial or final level of the sigmoid depending on whether b is positive or negative. A least squares linearized inversion method was used to determine the fit (a = 1.400, b = 0.016, c = 590.0, d = −0.980). Then, a uniform shift was applied to the measurements and the fit to give 99% of full coupling (e.g., $\log_{10}$ coupling = −0.004) for a source depth h which is just deep enough that the elastic sphere is entirely below the water table. That source depth is ~1750 m, which corresponds to an elastic radius of 1110 m (thus, $h - r_e$ = 640 m). Measurements and the coupling curve for surface waves, after making the shift, are plotted in Figure 9.

[44] These results may be compared with estimates of *Springer* [1966] for tuff and alluvium, and summaries for a

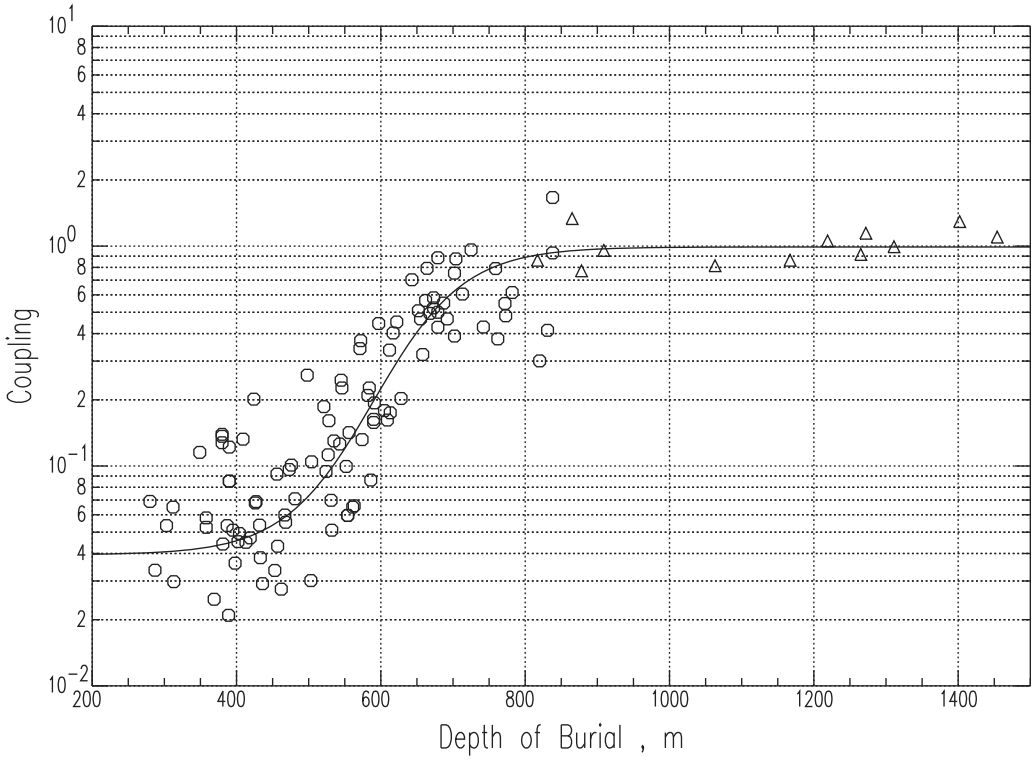

Figure 9. Coupling factors for Rayleigh (open triangles) and *Lg* waves (open circles) from the studies by *Taylor* [1982] and *Jones and Taylor* [1996]. A uniform shift has been applied to these measurements and the fit shown by the line. A nonlinear least squares method was used to obtain a fit to the measurements shown.

variety of media by *Murphy* [1996], where both studies are for *P* wave coupling. Surface wave coupling factors for source depths shallower than 600 m are somewhat lower than *P* wave estimates. The reason is that *P* wave coupling estimates weight the downgoing rays more heavily than surface waves which require a free surface for their existence. As such, the downgoing energy encounters water-saturated media where coupling improves, while surface waves sample the integrated effects of rays leaving at all take-off angles.

[45] The surface wave coupling curve was multiplied into the result for full coupling (green line in Figure 8), and the revised M_t estimate is plotted with a red line in Figure 8. For the benefit of closer scrutiny, K values and ratios $\hat{M}_I/M_t$ are plotted for a depth range between 400 and 1000 m in Figure 10.

[46] Plotted with the K measurements in Figure 10 is a sigmoid function that was fit by a nonlinear least squares method. This fit involved measurements for the entire Pahute Mesa data set as well as a few Rainier Mesa explosions with depths of ~400 m and less. Assuming a power law model for $\hat{M}_I/M_t$ ratios, three models are plotted with different exponents on K for the sigmoid function. We favor models with exponents between 1.0 and 1.5 mainly due to better fits to the ratios for depths between 600 and 700 m and their asymptotic values (0.74 and 0.64, respectively) are still consistent with the data scatter for the deepest shots. The purpose of these models is to illustrate the correlation between K values and the moment ratios with very simple models, while admittedly there is no reason to expect that a power law model is appropriate.

7. Extension of the Source Model to General Double-Couple Mechanisms

[47] Relaxation of tectonic prestress does not have to occur in a manner consistent with strike-slip faulting, as was assumed for the source model in equations (4) and (6). Relaxation consistent with dip-slip reverse faulting has been proposed for explosions at NTS and the Semipalatinsk Test Site (STS) [e.g., *Douglas and Rivers*, 1988; *Given and Mellman*, 1986]. PT08 argued that tectonic stresses are second order compared to stress glut related to the dynamics of free surface interactions and shock wave rebound. Nevertheless, it is of interest to investigate a contribution to the radiated wavefield for induced tectonic dip-slip motions. A new formula for K can be derived for a general double-couple mechanism based on the formulation of *Ekström and Richards* [1994] involving strike-slip (*SS*) and dip-slip (*DS*) motions

$$M_{xx} = M_I - 0.5 \cdot M_{CLVD} - SS \cdot \sin(2\phi) - 2DS \cdot (\sin(\phi))^2$$

$$M_{yy} = M_I - 0.5 \cdot M_{CLVD} + SS \cdot \sin(2\phi) - 2DS \cdot (\cos(\phi))^2$$

$$M_{zz} = M_I + M_{CLVD} + 2DS \quad M_{xy} = SS \cdot \cos(2\phi) + DS \cdot \sin(2\phi), \tag{15}$$

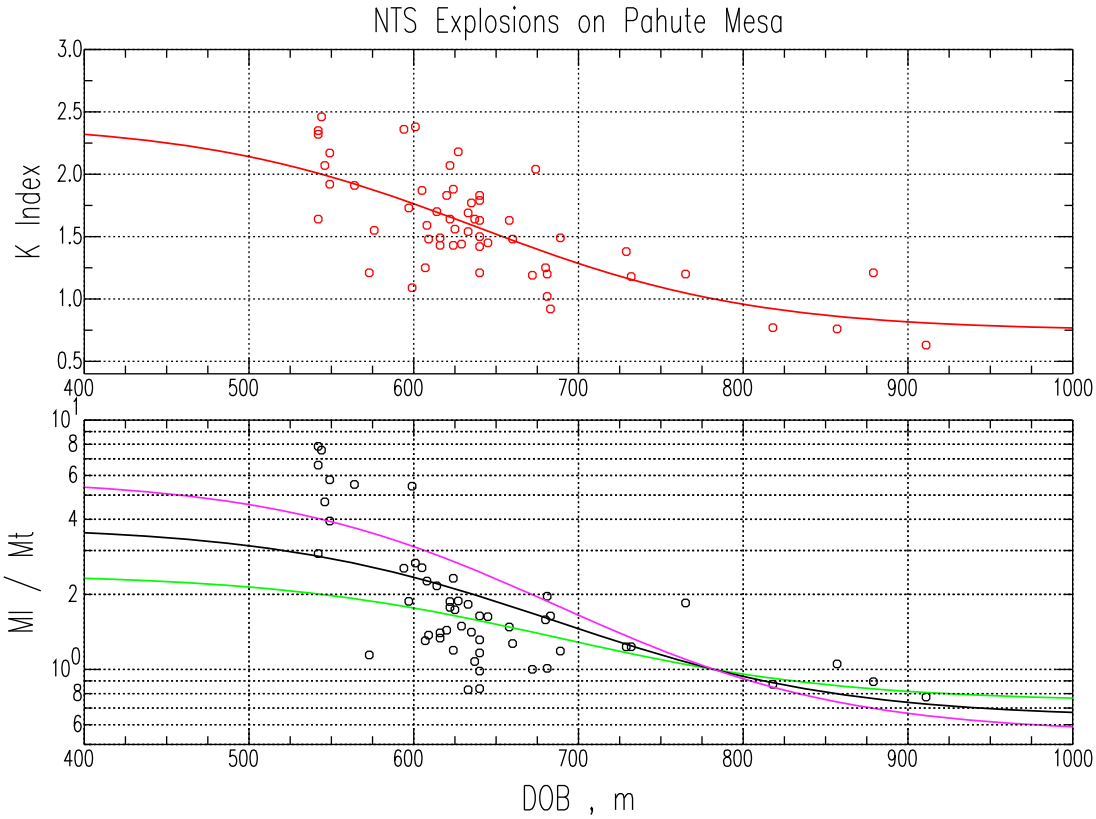

Figure 10. (top) K values from moment tensor inversions and a sigmoid fit. (bottom) Moment ratios $\hat{M}_I/M_t$ computed using the relationship for M_t adjusted for the effects of coupling (red line in Figure 8). Also shown with the ratios are power law models: $K^{1.0}$ (green), $K^{1.5}$ (black), and $K^{2.0}$ (magenta) using the sigmoid function in the top figure. Both Figures 10 (top) and 10 (bottom) are plotted in a restricted depth range to enable closer inspection.

where

$$SS \equiv M_0 \sin\delta\cos\lambda \quad DS \equiv \frac{1}{2} M_0 \sin\delta \sin\lambda, \tag{16}$$

for tectonic release with moment M_0, slip angle λ, and dip angle δ. M_{xz} and M_{yz} are functions of M_0, SS, DS, and ϕ, but are unconstrained by long-period surface wave observations due to their poor excitation characteristics for shallow sources. The inability to resolve these moment tensor elements for explosion sources has no impact on K for this model nor the model in equation (4) used for Pahute Mesa explosions as can be seen from its definition in equation (5) and the fact that the CLVD source is assumed to have a vertical axis of symmetry. Substituting the formulas for M_{xx}, M_{yy}, and M_{zz} above into equation (5), the new formula for K is

$$K' = \frac{2(M_I + M_{CLVD} + 2DS)}{(2M_I - M_{CLVD} - 2DS)}, \tag{17}$$

where a prime mark is used to distinguish it from the K for pure strike-slip release in equation (6). *Patton* [2010] analyzed the impact of a DS contribution in the context of *Ekström and Richards*'s [1994] results for STS explosions. Due to the fact that M_I is expected to increase after accounting for damage, it can be shown that $M_I + M_{CLVD} \gg 2max\{DS\}$ and $2M_I - M_{CLVD} \gg 2max\{DS\}$, where $max\{DS\}$ is the maximum expected value of DS based on the level of tectonic release F. This result applies to the full range of F values estimated on STS explosions. This means that K and K' are approximately equal even for large releases of tectonic strain energy. *Patton*'s [2010] study also showed that F values can be significantly overestimated for source models that do not include the effects of source medium damage.

8. Estimation of Yield: Depth of Burial Trade-Off Curves for the 2006 North Korean Test

[48] In the absence of significant radiation from damage, the measured isotropic moment should be related to yield through cavity radius scaling using classical theory for an incompressible source region. PT08 showed that m_b-M_s values for the 2006 North Korean test are consistent with a pure explosion source with negligible moment contributions from damage or tectonic release. While material damage undoubtedly occurred on this test, there was no expression of it in the radiated seismic waves at long periods. As such, this explosion provides an excellent opportunity to test the consistency of yield estimates based on $\hat{M}_I$ and m_b in order to show that, in principle, a deeper understanding of explosion moment holds promise to rectify the difficulties with past $\hat{M}_I$-W correlations [*Given and Mellman*, 1986;

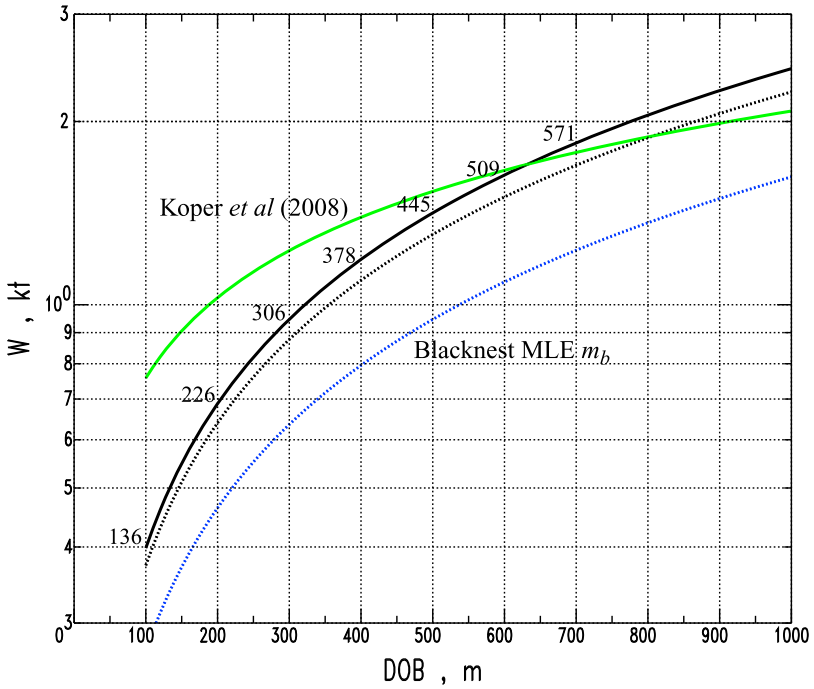

Figure 11. Yield versus depth of burial trade-off curves for the 2006 North Korean test. Curves plotted with a solid line are based on an isotropic moment $\hat{M}_I$ of 3×10^{14} Nm. The results from *Koper et al.* [2008] and equation (18) of this study are shown by green and black curves, respectively. The black dotted curve is based on m_b using a value of 4.08 and equation (20), while the blue dotted curve is based on Blacknest's MLE m_b. Scale depths of burials (h/W$^{1/3}$ in units of m per kt$^{1/3}$) are provided on the $\hat{M}_I$ curve from this study.

Ekström and Richards, 1994]. Here we follow a procedure similar to one used by *Koper et al.* [2008] to develop trade-off curves between yield and depth of burial for the 2006 test. However, the difference between our approach and the one taken by *Koper et al.* [2008] is that we set $\hat{M}_I$ equal to M_t in equation (10) whereas *Koper et al.* [2008] used DJ91's equation (41) for $\hat{M}_I$ which was calibrated against explosions that suffered source medium damage. The insights gained from the present paper and PT08 indicate that equation (41) is not the proper relationship to use for the 2006 North Korean test nor the 2009 test.

[49] Using the DJ91 r_c scaling relationship (see DJ91, equation 39) to compute V_c, the formula for M_t is

$$M_t = 4.42 \times 10^{12} \cdot \frac{1-\nu}{1-2\nu} \cdot \rho^{0.2125} \cdot \beta^{0.8456} \cdot h^{-0.7875} \cdot 10^{-0.0075GP} \cdot W, \quad (18)$$

in Nm, where ν is Poisson ratio and GP is percent gas porosity, and other parameters are in MKS units. For m_b, we adopt the empirical hard rock magnitude yield formula of *Ringdal et al.* [1992] ($m_b = 0.75 \cdot \log[W] + 4.45$). Assuming this formula holds for standard burial practice (i.e., 120 m/kt$^{1/3}$), a correction term for nonstandard burial depths using DJ91 scaling is

$$-0.7875 \cdot \log\left[h/\left(120W^{1/3}\right)\right], \quad (19)$$

and the m_b-W formula becomes

$$m_b = 1.0125 \cdot \log[W] - 0.7875 \cdot \log[h] + 6.09. \quad (20)$$

We chose the same medium parameter values for the North Korean test as *Koper et al.* [2008] did (α = 5100, β = 3000 m/s; ν = 0.23545; ρ = 2500 kg/m^3; GP = 0.5%). The measured moment is 3×10^{14} Nm [*Walter et al.*, 2007; *Koper et al.*, 2008]. For m_b, we took an average of magnitudes reported by the National Earthquake Information Center (NEIC; 4.2), the International Data Center (IDC; 4.1), and the United Kingdom's National Data Center at Blacknest (3.94 [*Selby and Bowers*, 2007]), e.g., (4.2 + 4.1 + 3.94)/3 = 4.08. Blacknest's m_b is a maximum likelihood estimate (MLE). Substituting these values of medium parameters and measurements into equations (18) and (20), and solving for yield, the following trade-off curves between depth of burial and yield are obtained

$$W = 0.0103 \cdot h^{0.7875}, \quad (21)$$

based on $\hat{M}_I$ and

$$W = 0.0104 \cdot h^{0.7778}, \quad (22)$$

based on m_b. These two trade-off curves are plotted in Figure 11.

[50] Also plotted in Figure 11 are the trade-off curve from *Koper et al.* [2008] based on $\hat{M}_I$ and a curve based on the

Blacknest MLE m_b. The difference between the former curve and the result in equation (21) is due to the fact that *Koper et al.* [2008] employed equation (41) of DJ91 which relates $\hat{M}_I$ and M_t through an additional factor related to overburden and gas porosity of the medium. DJ91 used explosions that suffered source medium damage to calibrate this equation, while damage appears not to be a significant source for the 2006 Korean test. A better physical basis of the source is the reason why we chose to use equation (18). Due to the small size of this NK test, one might expect Blacknest's MLE m_b to be a better estimate than those reported by NEIC or IDC. If so, the agreement with the moment-based trade-off curve is not as good as the trade-off curve based on average m_b. Nevertheless, in both cases, agreement is well within a factor of two and excellent for average m_b.

[51] It is gratifying to see fairly good agreement between trade-off curves based on m_b and an $\hat{M}_I$ trade-off curve grounded in a physical basis of the source. This is the promise that a better understanding of source physics holds for new $\hat{M}_I$-W relationships that give better agreement with m_b than past experience has shown. The trade-off curve based on Blacknest's m_b does remind us, however, that even with complete understanding of the explosion source, accurate yield estimation still requires reliable knowledge of near-source velocity structure and regional propagation effects. To derive equations (21) and (22), we had to assume values for the material properties in equation (18) and a negligible upper mantle bias on m_b, respectively. Preliminary analysis of the larger 2009 NK test, for which uncertainties on m_b are not as big of a concern, show results more like those for the Blacknest curve in Figure 11. A future paper will investigate systematic differences between m_b- and moment-based trade-off curves for the NK tests due to source medium structure and m_b bias.

[52] It should be noted that the depth dependencies are practically the same for trade-off curves in equations (21) and (22). Had they been different, there would have been some benefit from combining $\hat{M}_I$ and m_b estimates since the intersection of the curves would potentially reveal information about depth of burial and hence yield. This analysis brings out the potential of multiphase yield estimation if, for example, the dependence of S wave generation on depth of burial (or yield) proves to be considerably different.

9. Discussion

[53] The results in Figures 8 and 10 are consistent with the hypothesis that source medium damage is contributing a volumetric source above and beyond cavity formation for explosions on Pahute Mesa. The interpretation of K's steady decrease with yield approaching values of 1 or smaller and the implications for long-period radiation are confirmed by the general agreement between $\hat{M}_I$ and M_t estimates for the largest tests. Meanwhile, $\hat{M}_I$ becomes significantly larger than M_t for smaller, shallower tests. $\hat{M}_I$ up to 8 times larger than M_t estimates are seen, suggesting a larger volumetric source for damage compared to the moment release from cavity formation. This much moment release is not surprising in light of the order-of-magnitude estimates of *Ben-Zion and Ampuero* [2009] and recent high-resolution observations of earthquake-related damage [*Wu et al.*, 2009, 2010].

[54] K values for explosions in hard rock at the STS are expected to be larger than in weak rock due to effects of shear dilatancy [*Heuzé et al.*, 1991] and a stronger upward propagating shock wave which can be reinforced by shallower burial practices and a water table close to the free surface. On the other hand, K for STS explosions should show weaker yield dependence than NTS explosions since less compaction occurs in stronger materials like granite, and the threshold at which slapdown significantly reduces dilation of the source medium is expected to be at higher yields. Analyses we have carried out on measurements of the source term U_1 for Rayleigh waves from STS explosions (see *Ekström and Richards* [1994] for the definition of U_1) predict dependencies of K on m_b which are consistent with a stronger CLVD source and weaker yield dependence [*Patton*, 2010]. For these reasons, we believe that omission of source medium damage in previous source models for surface waves led to systematic errors in $\hat{M}_I$ which will account for poor correlations with yield.

[55] Results of this study and of PT08 predict that $\log[\hat{M}_I]$ and M_s for underground explosions might not scale 1 to 1, as they do for earthquakes [e.g., *Ekström and Dziewonski*, 1988]. The reason is that at lower yields, the effects of the CLVD source will tend to reduce M_s, while $\log[\hat{M}_I]$ is larger than $\log[M_t]$ due to the effects of source medium dilation, as seen in Figure 10. Both effects are expected to be muted at high yields. On a plot of $\log[\hat{M}_I]$ (x axis) versus M_s (y axis), data points at lower yields move to the right ($\hat{M}_I$ is larger) and down (M_s decreases), giving a slope greater than one. Regression analysis on a compilation of $\log[\hat{M}_I]$-M_s observations for nuclear explosions is consistent with this prediction [*Patton*, 2001, see Figure 4.5]. For a smaller ensemble made up of just Pahute Mesa explosions, linear regression of $\log[\hat{M}_I]$ versus MLE M_s values reported by *Stevens and Murphy* [2001] gives a slope of 1.18 ± 0.05 in good agreement with 1.12 ± 0.04 from *Patton* [2001].

[56] Discrepancies between close-in observations of reduced displacement potential $\psi(\tau)$ and far-field Rayleigh wave measurements of $\hat{M}_I$ led *Aki et al.* [1974, pp. 131 and 133] to identify an "outstanding problem" where "only about 1/3 of the residual potential [$\psi(\infty)$ observed close-in] is transmitted to the far-field at long periods." To explain the discrepancy, *Aki et al.* [1974] provided evidence for $\psi(\tau)$ with large overshoot, which was not observed for close-in ground motions due to their short durations of recording. They asserted that large overshoot results from the dynamics of the explosion source related to material compaction from spall slapdown. Our explanation for K decreasing with W is similar to this one. But we think that compaction due to spall slapdown must first overcome the effects of source medium dilation, and this is not expected for explosions with m_b less than 5.6, which were the focus of the discrepancy.

[57] *Murphy* [1974] used r_c scaling and equation (10) for an incompressible medium to show that Rayleigh wave measurements of $\hat{M}_I$ in the work by *Aki et al.* [1974] are consistent with an interpretation due to cavity creation for explosions in tuff. In other words, compaction of the source medium is not significant, contrary to *Aki et al.*'s [1974] assertion. *Murphy* [1974] points out that *Aki et al.* [1974] compare Rayleigh wave moments for explosions in tuff to close-in observations for hard rock explosions, and claims that the discrepancy is caused mainly by differences

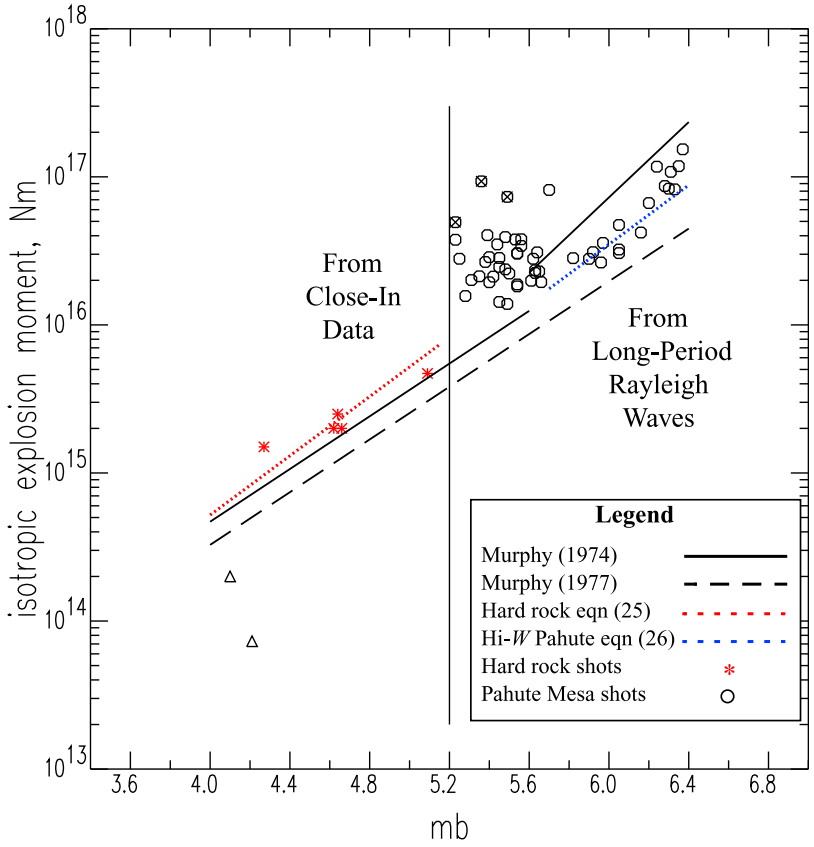

Figure 12. $\hat{M}_I$ plotted against m_b for explosions detonated in the western United States, with the exception of Salmon which was detonated in Hattiesburg, Mississippi. Figure 12 is an updated version of *Aki et al.* [1974, Figure 1]. Data points to the left of the vertical line are based on $\psi(\infty)$ obtained from close-in data, and five of the seven shots have updated m_b values (only Rainier and Gnome have the same m_b as reported by *Aki et al.* [1974]). Red stars are hard rock explosions, and black triangles are Rainier and Fisher, detonated in tuff and alluvium, respectively. $\hat{M}_I$ for Pahute Mesa explosions in this study have been corrected for the effects of seismic coupling and plot to the right of the vertical line. A circle-enclosed cross is used for the three shallowest Pahute Mesa explosions in the data set. Solid black lines are predictions from *Murphy* [1974]. Long-dashed line is based on the result of *Murphy* [1977], which includes a correction for compaction. The 1974 predictions were not corrected. Red dotted line is the average of DJ91 and *Heard and Ackerman* [1967] predictions from this study for the hard rock explosions and no compaction. The blue dotted line is analogous to the red but for deep, large Pahute Mesa explosions.

in acoustic bulk modulus between tuff and hard rock source media.

[58] Based on the results of this paper, an update of Figure 1 of *Aki et al.* [1974] and Figure 1 of *Murphy* [1974] is provided in Figure 12. As in the original figures, inferred isotropic moments based on $\psi(\infty)$ from close-in data plot to the left of the vertical line, while far-field Rayleigh wave moments $\hat{M}_I$ plot to the right of the line. Body wave magnitudes are taken from a recent Blacknest compilation (N. D. Selby et al., m_b: M_s event screening revisited, submitted to *Bulletin of the Seismological Society of America*, 2010) or from *Jih and Baumstark* [1994], with two exceptions noted in the caption of Figure 12. Of relevance to *Aki et al.*'s [1974] "outstanding problem" is the fact that updated magnitudes for five of the seven explosions with close-in data increased an average of 0.48 magnitude units. This much increase in m_b goes quite far to remove much of the discrepancy between close-in and far-field observations that first caught *Aki et al.*'s [1974] attention.

[59] In Figure 12, the far-field moments have been corrected for the effects of seismic coupling by taking $\hat{M}_I$ in Figure 8 and dividing by the sigmoid curve in Figure 9. We suspect that the shallowest explosions are somewhat overcorrected for the effects of seismic coupling. The close-in moments remain unchanged from *Aki et al.*'s [1974] paper. Reviews of free field data have been published over the years [e.g., *Perret and Bass*, 1975; *Murphy*, 1978, 1991], and revisions in $\psi(\infty)$ values have generally been relatively minor with the exception of Salmon. *Denny and Goodman* [1990] showed that $\psi(\infty)$ for Salmon was overestimated because ground motion data on which estimates of the potential were based were actually recorded in the nonlinear regime. Their estimate is 1.7 times smaller than *Aki et al.*'s [1974]; this change is by far the largest among revised estimates for other explosions. *Denny and Goodman* [1990] go on to claim that $\psi(\infty)$ for the other hard rock explosions in *Aki et al.*'s [1974] study are biased high for the same reasons, but they do not provide analysis to support their

claim. The one documented case for a significant change in $\psi(\infty)$ is compensated for on a plot of m_b versus moment. This is because Salmon was detonated in a stable region, while all other explosions in Figure 12 are located in the western United States where a hot upper mantle is known to reduce m_b. So a smaller $\psi(\infty)$ is offset by a needed reduction in Salmon's m_b in order to put it on par with the other explosions.

[60] The updated observations in Figure 12 show something completely different compared to *Aki et al.* [1974, Figure 1]. No longer is there any evidence whatsoever for their claim that only 1/3 of the residual potential observed close-in is transmitted to the far field. Instead, the intermediate size explosions on Pahute Mesa have far more isotropic moment than would be predicted by a simple extrapolation of the close-in observations to larger yields. This reversal in the close-in and far-field observations from what was observed in 1974 can be explained by excess moment due to damage if the close-in observations are consistent with predictions of M_t as was found in this study for the largest Pahute Mesa explosions.

[61] The M_t predictions of *Murphy* [1974] are plotted in Figure 12 as solid lines. Above 5.6 m_b, the prediction is too high because the r_c scaling relationship due to *Orphal* [1970] predicts too much cavity volume at large yields. Below 5.6 m_b, *Orphal*'s [1970] relationship does better based on comparisons with the scaling results in Figure 7. *Murphy* [1974] assumed no compaction for these predictions, while in the paper by *Murphy* [1977], a correction for compaction was applied to obtain the $\psi(\infty)$ scaling result in his equation (25). This correction was made with a simple multiplicative factor of 0.6 (MM71). The moment prediction based on this scaling for $\psi(\infty)$ and material properties adopted by *Murphy* [1974] for m_b less than 5.6 is also plotted in Figure 12 as a long-dashed line. As expected, it plots below his 1974 results due to the effect of compaction.

[62] Two more predictions, one for hard rock explosions and the other for large Pahute Mesa explosions, are also plotted in Figure 12. These predictions were obtained using equations (18) and (20) for the DJ91 model and a similar set of equations based on the *Heard and Ackerman* [1967] scaling model. The constant in equation (20) was reduced by 0.35 magnitude units in order to correct for test site bias. Then equation (20) was solved for W, and replacing W in equation (18), one obtains

$$M_t(\mathrm{DJ91}) \cong 7.58 \times 10^6 \cdot \rho^{0.2125} \cdot \alpha^{0.8456} \cdot 10^{m_b}, \qquad (23)$$

for a Poisson medium. Similarly, the following equation holds for the *Heard and Ackerman* [1967] model,

$$M_t(\mathrm{HA67}) \cong 1.23 \times 10^4 \cdot \rho^{0.13} \cdot \alpha^{1.7} \cdot 10^{m_b}. \qquad (24)$$

Both of these formulas are for incompressible media (i.e., no compaction). For the hard rock explosions, we chose density and velocity by taking the average of values reported for all five explosions, i.e., $\rho = 2400$ kg/m^3 and $\alpha = 4500$ m/s. The results are

$$M_t(\mathrm{DJ91}) = 4.9 \times 10^{10} \cdot 10^{m_b} \text{ and } M_t(\mathrm{HA67}) = 5.5 \times 10^{10} \cdot 10^{m_b} \qquad (25)$$

in Nm. Since these results were so close, only the average is plotted in Figure 12 as a red dotted line. The results for large, deep Pahute Mesa explosions are

$$M_t(\mathrm{DJ91}) = 3.8 \times 10^{10} \cdot 10^{m_b} \text{ and } M_t(\mathrm{HA67}) = 3.5 \times 10^{10} \cdot 10^{m_b} \qquad (26)$$

in Nm, where $\rho = 2000$ kg/m^3 and $\alpha = 3500$ m/s, which are the values adopted by *Murphy* [1974] for m_b greater than 5.6. See the blue dotted line in Figure 12.

[63] The good agreement between observations and predictions from equation (26) confirms what we already knew from the results in Figure 8: $\hat{M}_I$ for large Pahute Mesa explosions are well predicted by classical theory for cavity formation in an incompressible medium with no appreciable volumetric contribution from damage. Judging from the observations and predictions based on equation (25), the same appears to be true for the hard rock explosions. All five explosions (Salmon and Gnome in salt, Hardhat in granite, Handcar in dolomite, and Gasbuggy in shale) were overburied to some extent (475, 250, 161, 176, and 420 m/kt$^{1/3}$, respectively, from announced yields) and were the first explosions detonated at their respective sites. Except for the relatively low strength of their media, as indicated by source medium velocities (4500 versus ~5100 m/s), these explosions might serve as analogs to the NK tests. Weaker media may account for spall observed even on well-overburied explosions like Gasbuggy [*Murphy and Archambeau*, 1986], while no evidence for spallation is found on the NK tests [e.g., *Schlittenhardt et al.*, 2010]. Nevertheless, we suspect that damage phenomena related to free surface interactions, as illustrated in Figure 1, were suppressed on all of these shots, and consequently $\psi(\infty)$ values were largely influenced by volumetric effects due to cavity formation.

[64] It is extraordinary that large, normal-buried Pahute Mesa explosions and small, overburied explosions detonated in pristine, intact medium should have commonality in that their isotropic moments are predicted so well by classical theory. However, the reasons are very different in each case. For Pahute Mesa explosions, damage was extensive, but it contributes little to the long-period radiation because dilation of the surrounding source volume is reversed and reduced to low static levels at high yields by the impulse of spall slapdown compacting materials in the source region. Meanwhile, damage from free surface interactions is relatively small to start with for the small explosions due to intact, relatively high-strength media and burial depths large for the yield. As such, the expression of damage is unimportant in the radiated seismic waves at long periods compared to the direct effects of cavity formation.

10. Conclusion

[65] Source medium damage due to the explosion source can radiate seismic waves as volumetric, double couple, and compensated linear vector dipole (CLVD) body force systems. The implications of such radiation for source discrimination, yield estimation, and for the physical basis of shear wave generation are far reaching. A previous study [*Patton and Taylor*, 2008] demonstrated the significant impact of Rayleigh wave radiation from a CLVD source on M_s and the performance of the m_b-M_s discriminant. In the

current paper, we build on that study by exploring the possibility of long-period radiation from a volumetric source of damage. We tested a hypothesis that damage contributes to the volumetric source above and beyond the moment due to cavity formation and that the extent to which it adds (or subtracts) moment is controlled by material properties and the dynamics of stress wave rebound, shock wave interactions with the free surface, gravitational unloading, and subsequent slapdown of spalled near-surface layers. Comparisons of measured isotropic moments for Pahute Mesa explosions with moments estimated from classical theory for cavity formation alone are consistent with this hypothesis. For this reason, measured isotropic moment from explosions should be viewed as "apparent" explosion moment since, in general, it has contributions from direct effects of the explosion source (cavity formation) and indirect effects (nonlinear damage mechanisms). In contrast to NTS tests in weak media, explosions in hard rock are expected to suffer more from damage due to effects of shear dilatancy. Furthermore, an upward propagating shock wave can be made stronger by shallower burial practices and a water table close to the free surface, which are probably the conditions under which STS nuclear explosions were conducted. We think that attempts to use isotropic moment as an indicator of yield were unsuccessful due to the omission of source medium damage in previous source models. A better physical understanding of isotropic moment (1) shows why source medium damage should not be included for the 2006 North Korean test, (2) improves the agreement of trade-off curves between yield and depth of burial based on $\hat{M}_I$ and m_b, and (3) offers promising new $\hat{M}_I$ -W relationships. Preliminary indications are that, by ignoring the effects of damage, past investigations very likely deduced source models that overestimated the F value of the double-couple source. The extent to which damage radiates as a double couple has not been considered in this paper, but in our opinion it would not be surprising if it turns out to be relatively significant. Whatever the contribution from damage may be, the importance of tectonic release as a source of double-couple radiation from nuclear explosions will diminish.

[66] **Note added in proof.** Subsequent analysis of M_s-yield scaling relationships constrains the exponent on K in Figure 10 (bottom) to be greater than 0.2 and less than 1.0. Adopting an exponent of 0.5, the net volumetric moment due to direct (cavity formation) and indirect (source medium damage) effects is ~40% more than the moment due to cavity formation alone for a normal-buried explosion on Pahute Mesa with K value of 2.

[67] **Acknowledgments.** We thank M. Nafi Toksöz of the Massachusetts Institute of Technology for his probing question to us over 3 years ago concerning the long-period implications of a model that includes the effects of source medium damage. This question led to a series of discoveries by the authors culminating in this paper and the paper by *Patton and Taylor* [2008] concerning the impact on m_b-M_s discrimination. We would like to thank Paul Richards of Columbia University for taking interest in our work, for providing valuable feedback regarding assumptions about tectonic release in the paper by *Patton and Taylor* [2008], and for many helpful comments on a draft of this paper. Paul's feedback on the paper by *Patton and Taylor* [2008] led to the study by *Patton* [2010] and is still the subject of ongoing investigations. We also thank Yehuda Ben-Zion of the University of Southern California for insights into his recent work on damage related to earthquake sources and for comments on our work and Steven Day of San Diego State University and an anonymous reviewer for beneficial reviews of the manuscript. The work in this paper was performed under the auspices of the Department of Energy for the Los Alamos National Laboratory under contract DE-AC52-06BA25396.

References

Aki, K. (1966), Generation and propagation of G waves from the Niigata earthquake of June 16, 1964. 2. Estimation of earthquake movement, released energy, and stress-strain drop from G wave spectrum, *Bull. Earthquake Res. Inst.*, *44*, 23–88.

Aki, K., and M. Bouchon (1974), A reply to Murphy's "Discussion of "Seismic source function for an underground nuclear explosion" by Keiiti Aki, Michel Bouchon, and Paul Reasenberg," *Bull. Seismol. Soc. Am.*, *64*, 1599–1600.

Aki, K., and P. G. Richards (2002), *Quantitative Seismology*, 2nd ed., Univ., Sci., Sausalito, Calif.

Aki, K., M. Bouchon, and P. Reasenberg (1974), Seismic source function for an underground nuclear explosion, *Bull. Seismol. Soc. Am.*, *64*, 131–148.

App, F. N., and W. M. Brunish (1992), Modelling surface motion and spall at the Nevada Test Site, *Rep. LA-UR-92-0500*, Los Alamos Natl. Lab., Los Alamos, N. M.

Ashby, M. F., and C. G. Sammis (1990), The damage mechanics of brittle solids in compression, *Pure Appl. Geophys.*, *133*, 489–521, doi:10.1007/BF00878002.

Ben-Zion, Y., and J.-P. Ampuero (2009), Seismic radiation from regions sustaining material damage, *Geophys. J. Int.*, *178*, 1351–1356, doi:10.1111/j.1365-246X.2009.04285.x.

Bishop, R. H. (1963), Spherical shock waves from underground explosions, close-in phenomena of buried explosions, *Final Rep. SC-4907(RR)*, pp. 115–158, Sandia Corp., Albuquerque, N. M.

Boardman, C. R., D. D. Rabb, and R. D. McArthur (1964), Responses of four mediums to contained nuclear explosions, *J. Geophys. Res.*, *69*, 3457–3469, doi:10.1029/JZ069i016p03457.

Day, S. M., and K. L. McLaughlin (1991), Seismic source representations for spall, *Bull. Seismol. Soc. Am.*, *81*, 191–201.

Denny, M. D., and D. M. Goodman (1990), A case study of the seismic source function: Salmon and Sterling reevaluated, *J. Geophys. Res.*, *95*, 19,705–19,723, doi:10.1029/JB095iB12p19705.

Denny, M. D., and L. R. Johnson (1991), The explosion seismic source function: Models and scaling laws reviewed, in *Explosion Source Phenomenology*, *Geophys. Monogr. Ser.*, vol. *65*, edited by S. R. Taylor et al., pp. 1–24, AGU, Washington, D. C.

Douglas, A., and J. A. Hudson (1990), The effect on teleseismic *P* of the zone of damage created by an explosion, *Geophys. J. Int.*, *103*, 111–133, doi:10.1111/j.1365-246X.1990.tb01757.x.

Douglas, A., and D. W. Rivers (1988), An explosion that looks like an earthquake, *Bull. Seismol. Soc. Am.*, *78*, 1011–1019.

Ekström, G., and A. M. Dziewonski (1988), Evidence of bias in estimations of earthquake size, *Nature*, *332*, 319–323, doi:10.1038/332319a0.

Ekström, G., and P. G. Richards (1994), Empirical measurements of tectonic moment release in nuclear explosions from teleseismic surface waves and body waves, *Geophys. J. Int.*, *117*, 120–140, doi:10.1111/j.1365-246X.1994.tb03307.x.

Ferguson, J. F., A. H. Cogbill, and R. G. Warren (1994), A geophysical-geological transect of the Silent Canyon caldera complex, Pahute Mesa, Nevada, *J. Geophys. Res.*, *99*, 4323–4339, doi:10.1029/93JB02447.

Fischer, F., P. Papanek, and R. Hamilton (1972), The Massachusetts Mountain earthquake of 5 August 1971 and its aftershocks, *Rep. 474-149*, U.S. Geol. Surv., Menlo Park, Calif.

Ford, S. R., D. S. Dreger, and W. R. Walter (2009), Identifying isotropic events using regional moment tensor inversion, *J. Geophys. Res.*, *114*, B01306, doi:10.1029/2008JB005743.

Given, J. W., and G. R. Mellman (1986), Estimating explosion and tectonic release source parameters of underground nuclear explosions from Rayleigh and Love wave observations, *Final Rep., AFGL-TR-86–0171(I)*, part I, 70 pp., Air Force Geophys. Lab., Hanscom Air Force Base, Mass.

Heard, H. C., and F. J. Ackerman (1967), Prediction of cavity radius from underground nuclear explosions, *Rep. UCRL-50324*, Lawrence Radiat. Lab., Livermore, Calif.

Heuzé, F. E., T. R. Butkovich, O. R. Walton, and D. M. Maddix (1991), Explosion phenomenology in jointed rocks: New insights, in *Explosion Source Phenomenology*, *Geophys. Monogr. Ser.*, vol. 65, edited by S. R. Taylor et al., pp. 151–159, AGU, Washington, D. C.

Howard, N. W. (1985), Variation in properties of nuclear test areas and media at the Nevada Test Site, *Rep. UCRL-53721*, Lawrence Livermore Natl. Lab., Livermore, Calif.

Jih, R.-S., and R. R. Baumstark (1994), Maximum-likelihood network magnitude estimates of low-yield underground explosions, *Rep. TBE-4617-3/TGAL-94-02*, Teledyne-Brown Eng., Arlington, Va.

Johnson, L. R., and C. G. Sammis (2001), Effects of rock damage on seismic waves generated by explosions, *Pure Appl. Geophys.*, *158*, 1869–1908, doi:10.1007/PL00001136.

Jones, E. M., and S. R. Taylor (1996), Are *Lg* spectra from NTS self similar?, *Bull. Seismol. Soc. Am.*, *86*, 445–456.

Jones, E. M., F. N. App, and R. W. Whitaker (1993). Ground motions and the infrasound signal: A new model and the discovery of a significant cavity rebound signal, *Rep. LA-UR-93-0861*, Los Alamos Natl. Lab., Los Alamos, N. M.

Knopoff, L., and M. J. Randall (1970), The compensated linear-vector dipole: A possible mechanism for deep earthquakes, *J. Geophys. Res.*, *75*, 4957–4963, doi:10.1029/JB075i026p04957.

Koper, K. D., R. B. Herrmann, and H. M. Benz (2008), Overview of open seismic data from the North Korean event of 9 October 2006, *Seismol. Res. Lett.*, *79*, 178–185, doi:10.1785/gssrl.79.2.178.

Lay, T. (1991), The teleseismic manifestation of *pP*: Problems and paradoxes, in *Explosion Source Phenomenology*, *Geophys. Monogr. Ser.*, vol. 65, edited by S. R. Taylor et al., pp. 109–125, AGU, Washington, D. C.

Leonard, M. A., and L. R. Johnson (1987), Velocity structure of Silent Canyon caldera, Nevada Test Site, *Bull. Seismol. Soc. Am.*, *77*, 597–613.

Mal, A. K., and L. Knopoff (1967), Elastic wave velocities in two-component systems, *J. Inst. Math. Its Appl.*, *3*, 376–387, doi:10.1093/imamat/3.4.376.

Mueller, R. A., and J. R. Murphy (1971), Seismic characteristics of underground nuclear detonations, part I. Seismic spectrum scaling, *Bull. Seismol. Soc. Am.*, *61*, 1675–1692.

Müller, G. (1973), Seismic moment and long-period radiation of underground nuclear explosions, *Bull. Seismol. Soc. Am.*, *63*, 847–857.

Murphy, J. R. (1974), Discussion of "Seismic source function for an underground nuclear explosion" by Keiiti Aki, Michel Bouchon, and Paul Reasenberg, *Bull. Seismol. Soc. Am.*, *64*, 1595–1597.

Murphy, J. R. (1977), Seismic source functions and magnitude determinations for underground nuclear explosions, *Bull. Seismol. Soc. Am.*, *67*, 135–158.

Murphy, J. R. (1978), A review of available free-field seismic data from underground nuclear explosions in salt and granite, *Interim Tech. Rep., CSC-TR-78-0003*, Comput. Sci., Falls Church, Va.

Murphy, J. R. (1991), Free-field seismic observations from underground nuclear explosions, in *Explosion Source Phenomenology*, *Geophys. Monogr. Ser.*, vol. 65, edited by S. R. Taylor et al., pp. 25–33, AGU, Washington, D. C.

Murphy, J. R. (1996), Types of seismic events and their source descriptions, in *Monitoring a Comprehensive Test Ban Treaty*, edited by E. S. Husebye and A. M. Dainty, pp. 225–245, Kluwer Acad., Dordrecht, Netherlands.

Murphy, J. R., and C. B. Archambeau (1986), Variability in explosion body-wave magnitudes: An analysis of the Rulison/Gasbuggy anomaly, *Bull. Seismol. Soc. Am.*, *76*, 1087–1113.

Orphal, D. L. (1970), The cavity formed by a contained underground nuclear detonation, *Rep. NVO-1163-TM-15*, Environ. Res. Corp., Alexandria, Va.

Patton, H. J. (1982), Measurements of Rayleigh-wave phase velocities in Nevada: Implications for explosion sources and the Massachusetts Mountain earthquake, *Bull. Seismol. Soc. Am.*, *72*, 1329–1349.

Patton, H. J. (1988), Source models of the Harzer explosion from regional observations of fundamental-mode and higher-mode surface waves, *Bull. Seismol. Soc. Am.*, *78*, 1133–1157.

Patton, H. J. (1990), Characterization of spall from observed strong ground motions on Pahute Mesa, *Bull. Seismol. Soc. Am.*, *80*, 1326–1345.

Patton, H. J. (1991), Seismic moment estimation and the scaling of the long-period explosion source spectrum, in *Explosion Source Phenomenology*, *Geophys. Monogr. Ser.*, vol. 65, edited by S. R. Taylor et al., pp. 171–183, AGU, Washington, D. C.

Patton, H. J. (2001), Regional magnitude scaling, transportability, and M_s:m_b discrimination at small magnitudes, *Pure Appl. Geophys.*, *158*, 1951–2015, doi:10.1007/PL00001138.

Patton, H. J. (2010), Explosion source model development in support of seismic monitoring technologies: Apparent explosion moment and prospects for moment-based yield estimation, paper presented at 2010 Monitoring Research Review: Ground-Based Nuclear Explosion Monitoring Technologies, Air Force Res. Lab., Orlando, Fla.

Patton, H. J., and S. R. Taylor (2008), Effects of shock-induced tensile failure on m_b-M_s discrimination: Contrasts between historic nuclear explosions and the North Korean test of 9 October 2006, *Geophys. Res. Lett.*, *35*, L14301, doi:10.1029/2008GL034211.

Patton, H. J., J. L. Bonner, and I. N. Gupta (2005), *Rg* excitation by underground explosions: Insights from source modelling the 1997 Kazakhstan depth-of-burial experiment, *Geophys. J. Int.*, *163*, 1006–1024, doi:10.1111/j.1365-246X.2005.02752.x.

Perret, W. R., and R. C. Bass (1975), Free-field ground motion induced by underground explosions, *Tech. Rep. SAND74-0252*, Sandia Natl. Lab., Albuquerque, N. M.

Richards, P. G., and W.-Y. Kim (2005), Equivalent volume sources for explosions at depth: Theory and observations, *Bull. Seismol. Soc. Am.*, *95*, 401–407, doi:10.1785/0120040034.

Ringdal, F., P. D. Marshall, and R. W. Alewine (1992), Seismic yield determination of Soviet underground nuclear explosions at the Shagan River test site, *Geophys. J. Int.*, *109*, 65–77, doi:10.1111/j.1365-246X.1992.tb00079.x.

Schlittenhardt, J., M. Canty, and I. Grünberg (2010), Satellite Earth observations support CTBT monitoring: A case study of the nuclear test in North Korea of Oct. 9, 2006 and comparison with seismic results, *Pure Appl. Geophys.*, *167*, 601–618, doi:10.1007/s00024-009-0036-x.

Selby, N. D., and D. Bowers (2007), Implications of the 9 October 2006 North Korean nuclear test for event screening, *Seismol. Res. Lett.*, *78*(2), 253.

Sharpe, J. A. (1942), The production of elastic waves by explosion pressures. I. Theory and empirical field observations, *Geophysics*, *7*, 144–154, doi:10.1190/1.1445002.

Springer, D. L. (1966), *P*-wave coupling of underground nuclear explosions, *Bull. Seismol. Soc. Am.*, *56*, 861–876.

Springer, D. L., G. A. Pawloski, J. L. Ricca, R. F. Rohrer, and D. K. Smith (2002), Seismic source summary for all U.S. below-surface nuclear explosions, *Bull. Seismol. Soc. Am.*, *92*, 1806–1840, doi:10.1785/0120010194.

Stevens, J. L., and S. M. Day (1985), The physical basis of m_b:M_s and variable frequency magnitude methods for earthquake/explosion discrimination, *J. Geophys. Res.*, *90*, 3009–3020, doi:10.1029/JB090iB04p03009.

Stevens, J. L., and J. R. Murphy (2001), Yield estimation from surface-wave analysis, *Pure Appl. Geophys.*, *158*, 2227–2251, doi:10.1007/PL00001147.

Stevens, J. L., G. E. Baker, H. Xu, T. J. Bennett, N. Rimer, and S. M. Day (2003), The physical basis of *Lg* generation by explosion sources, paper presented at the 25th Seismic Research Review—Nuclear Explosion Monitoring: Building the Knowledge Base, Natl. Nucl. Secur. Admin., Tucson, Ariz.

Taylor, S. R. (1982), Calculation of seismic coupling factors at NTS from inversion of regional amplitudes, *Earthquake Notes*, *53*(1), 8.

Taylor, S. R. (2009), Can the Fisk conjecture be explained by rock damage around explosions?, *Bull. Seismol. Soc. Am.*, *99*, 2552–2555, doi:10.1785/0120080332.

Toksöz, M. N., and H. H. Kehrer (1972), Tectonic strain release by underground nuclear explosions and its effect on seismic discrimination, *Geophys. J. R. Astron. Soc.*, *31*, 141–161.

U.S. Department of Energy (1995), Caging the dragon: The containment of underground nuclear explosions, *Rep. DOE/NV-388*, 726 pp., Las Vegas, Nev.

Vergino, E. S., and R. W. Mensing (1990), Yield estimation using regional m_b(Pn), *Bull. Seismol. Soc. Am.*, *80*, 656–674.

Viecelli, J. A. (1973), Spallation and the generation of surface waves by an underground explosion, *J. Geophys. Res.*, *78*, 2475–2487, doi:10.1029/JB078i014p02475.

Wallace, T. C. (1991), Body wave observations of tectonic release, in *Explosion Source Phenomenology*, *Geophys. Monogr. Ser.*, vol. *65*, edited by Taylor, S. R. et al., pp. 161–170, AGU, Washington, D. C.

Walter, W. R., E. Matzel, M. E. Payanos, D. B. Harris, R. Gok, and S. R. Ford (2007), Empirical observations of earthquake-explosion discriminants using *P/S* ratios and implications for the sources of explosion *S*-waves, paper presented at the 29th Monitoring Research Review: Ground-Based Nuclear Explosion Monitoring Technologies, Natl. Nucl. Secur. Admin., Denver, Colo.

Wu, C., Z. Peng, and Y. Ben-Zion (2009), Non-linearity and temporal changes of fault zone site response associated with strong ground motion, *Geophys. J. Int.*, *176*, 265–278, doi:10.1111/j.1365-246X.2008.04005.x.

Wu, C., Z. Peng, and Y. Ben-Zion (2010), Refined thresholds for nonlinear ground motion and temporal changes of site response associated with medium size earthquakes, *Geophys. J. Int.*, *182*, 1567–1576, doi:10.1111/j.1365-246X.2010.04704.x.

H. J. Patton, Los Alamos National Laboratory, Los Alamos, NM 87545, USA. (patton@lanl.gov)

S. R. Taylor, Rocky Mountain Geophysics, Los Alamos, NM 87544, USA.